BCSJ

Accounts

Nature-Inspired Design of Smart Biomaterials Using the Chemical Biology of Nucleic Acids

Ganesh N. Pandian[1] **and Hiroshi Sugiyama***[1,2]

[1]Institute for Integrated Cell-Material Sciences (WPI-iCeMS), Kyoto University, Yoshida-Ushinomaecho, Sakyo-ku, Kyoto 606-8501

[2]Department of Chemistry, Graduate School of Science, Kyoto University, Kitashirakawa-Oiwakecho, Sakyo-ku, Kyoto 606-8502

E-mail: hs@kuchem.kyoto-u.ac.jp

Received: February 23, 2016; Accepted: March 18, 2016; Web Released: August 15, 2016

Ganesh N. Pandian

Ganesh N. Pandian received his Ph.D. in Biotechnology in 2009 from Niigata University under Prof. Hidetaka Hori with a Monbukagakusho (Japanese Government) scholarship. He continued his research with Prof. Hori as Assistant Professor (Research). He is now working as Assistant Professor at the Institute for Integrated Cell-Material Sciences (WPI-iCeMS), Kyoto University with Prof. Hiroshi Sugiyama. His current research focus is to develop nature-inspired smart biomaterials.

Hiroshi Sugiyama

Hiroshi Sugiyama received his Ph.D. in 1984 with Teruo Matsuura at Kyoto University. After postdoctoral studies at the University of Virginia with Sidney M. Hecht, he returned to Kyoto University in 1986 as an Assistant Professor and became an Associate Professor in 1993. In 1996 he joined Institute of Biomaterials and Bioengineering at Tokyo Medical and Dental University. He has been a Professor of Chemical Biology at Kyoto University since 2003. Among the honors he has received are the Nippon IBM Award and the Chemical Society of Japan Award for Creative Work.

Abstract

In the natural cellular environment, nucleic acid biomolecules like DNA have biological implications via structural modifications and through precise coordination with other biomolecules in the local environment. Here, we detail the design of nature-inspired smart biomaterials that are based on the chemical biology of nucleic acids. *N*-Methylpyrrole (P) and *N*-methylimidazole (I) polyamides (PIPs), sequence-specific DNA-binding molecules have been, developed to image specific DNA sequences and to alter gene expression inside the living cells. The self-assembling feature of DNA was harnessed to achieve the programmed assembly of nanostructures with different dimensions. Also, the advanced DNA architectures with well-defined properties allowed the real-time visualization of the complicated single-molecule interactions, which in-turn provided vital intracellular mechanistic information. The molecular recognition properties of DNA were exploited to design biologically inspired hybrid catalysts for sustainable organic synthesis. Our review could serve as a guidebook for researchers who aim to develop nucleic acid-based synthetic biomaterials.

1. Introduction

Information is a powerful resource that needs to be managed to avoid aberrant manifestations and has to be harnessed in a meticulous manner. In nature, living organisms manage their biological information remarkably by organizing it in a timely manner.[1] The informational molecule called deoxyribonucleic acid (DNA) stores and retrieves genetic information at the right place and time in all living systems. Friedrich Miescher first identified DNA as nuclein in 1869. In 1953, Watson and Crick found that DNA in living organisms is found as a pair of molecules in the shape of a double helix and not as a single biomolecule.[2] Since the discovery of the double-helix structure

of the DNA, an ever-increasing amount of genetic information is being generated. Several incurable diseases can now be understood at the level of molecular DNA.[3] Consequently, genetic-knowledge-based therapeutic strategies for treating diseases have been gaining attention in the medical field.[4] Transcription factors (TFs) govern the fate of prokaryotic and eukaryotic cells by transcribing precisely the biological information from DNA to construct cellular components. A malfunction in the intricate machinery of TFs has been correlated with a growing number of human diseases.[5]

Natural TFs have flexible structures and are composed of three domains: (i) a DNA-binding domain (DBD) that attaches to specific enhancer or promoter sequences; (ii) a linker domain (LD); and (iii) a transcriptional activation domain (TAD) that contains binding sites for other proteins.[6] Therefore, artificial transcription factors (ATFs) that restore the expression of genes that are perturbed in disease are attractive as potential therapies. The past decade has seen the active development of synthetic modulators that are capable of transcriptional activation.[7] Nevertheless, for effective transcriptional regulation, there is a demand to develop smart biomaterials, such as DNA-based ATFs, that mimic the structure of TFs and retain the capacity of their natural counterparts to partake in intricate gene-regulatory networks. DNA molecules are packaged into nucleosomes, which are highly compacted structures in which DNA strands are wrapped around histones. Two key regulatory processes govern the "ON" and "OFF" states of gene expression in vivo. One is related to the base sequences that mediate the binding of transcription factors to promoter regions. The other is related to the epigenetic control that results from changes in nucleosome structure after acetylation, methylation, and other histone modifications. DNA possesses a considerable conformational flexibility, such as the A-form, Z-form, and G-quadruplex.[8] Such structural changes in DNA often control the transcriptional status of a cell. This dynamic nature of gene expression complicates the effective transcriptional activation of a gene of interest. In this regard, there is a need to integrate fragmented knowledge stemming from various disciplines and devise a sustainable strategy for efficient gene modulation. This overarching goal may be achieved via in-depth analysis of the major biological mechanisms occurring around local DNA structures. Such vital mechanistic insights may be gained by building nano- and meso-sized structures with high precision.

To achieve such a complex feat, the remarkable self-assembling feature and the precise recognition ability of DNA should be harnessed to construct desired structures with biochemical importance. DNA can assemble molecules and nanomaterials in a programmable manner because of its precise base-pairing system and programmable linear sequence, which allow an exclusive association via the use of four bases (A, C, G, and T) and two base pairs (AT and CG). Double-stranded DNA also allows the design of predicted structures because of its well-characterized right-handed helical structure and periodic geometry (the 10–10.5 base pairs per turn and 0.34 nm distance between neighboring base pairs).[9] Modern synthetic chemistry allows the production of hundreds of different DNA molecules, whereas chemical DNA synthesis processes have an advantage regarding what is observed in a biological system, as these technologies allow the incorporation of targeting small molecules directly and their site-selective introduction into a DNA strand. DNA may also be altered to encompass diverse functional molecules, fluorescent molecules, and nanomaterials and can be biochemically manipulated using modifying enzymes, such as DNA ligase, kinases, polymerases, and restriction enzymes. Oligodeoxyribonucleotides represent the primary class of molecules for the preparation of functional modules and scaffolds and for the placement of functional molecules and nanomaterials. Functionalized oligonucleotides can be used in template-directed organic synthesis processes and for performing unusual chemical reactions.[10] DNA–gold nanoparticle conjugates may be used for the sensitive detection of a target DNA.[11] The controlled self-assembly and nanostructure of DNA bestow unique functionalities, particularly when the conjugated units are assembled sequentially. The naturally occurring self-assembly feature of DNA has inspired scientists to simulate the phenomenon for the construction of functional materials. As controlled self-assembly may yield important structures, bottom-up approaches based on self-assembly are in demand.[12] To accomplish this complex feat, a precise control of programming predesigned structures and the placement of functional molecules into defined scaffolds are needed. Moreover, the intrinsic flexibility of long DNA chains should be controllable via the incorporation of specially designed structures to construct informative biomaterials.

Furthermore, DNA is an attractive chiral source for asymmetric synthesis. Because of its high solubility in water, DNA is considered suitable for the development of water-compatible catalysts that induce and control enantioselectivity.[13] As an innovative approach, we integrated DNA nanotechnology, cell biology, and synthetic organic chemistry techniques to acquire vital mechanistic information and develop knowledge-based smart functional biomaterials.

2. Development of Innovative DNA-Based Sequence-Specific Small Molecules as Artificial Genetic Switches

Genomic DNA carries a huge amount of information using only four nucleobases (bases). Consequently, small molecules or natural proteins that interact with these bases may alter significantly cellular functions and phenotypes. Accordingly, the oligopeptide antibiotics netropsin and distamycin A inhibit nucleic acid synthesis depending on the base composition of the template DNA.[14] Dickerson et al. solved the crystal structure of netropsin bound to the nucleotide sequence d(CGCGAATTCGCG) and proposed that the substitution of imidazole (I) for pyrrole (P) in netropsin generates a class of small molecules that can read G/C-containing base sequences.[15] A DNA minor-groove-binding peptide that reads the sequence (5′–(A, T)GCGC(A, T)–3′) suggested the formation of a 2:1 positively cooperative complex with a four-ligand (IPPI). Aliphatic/aromatic amino acid pairings facilitated the design of hairpin polyamides with a wider and more diverse sequence-recognition ability, and NMR studies corroborated the importance of the γ-amino butyric acid turn in improving sequence selectivity.[16] Therefore, a binding rule was proposed that stated that antiparallel pairing of I opposite P (I/P) recognizes a G–C base pair, whereas a P/P pair recognizes A–T or T–A base pairs (Figure 1).[17] Hairpin pyrrole-imidazole polyamides (PIPs) possess binding constants and sequence specific-

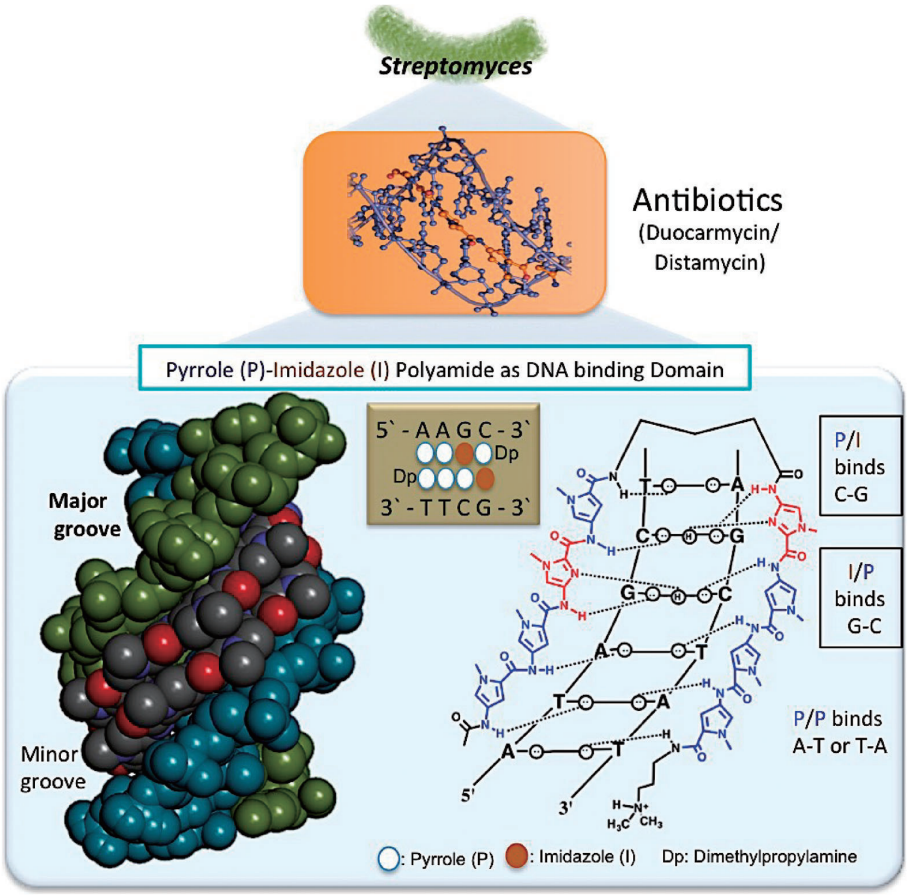

Figure 1. Illustration of pyrrole-imidazole polyamides development as DNA-binding domain from the antibiotics that were derived from bacteria Streptomyces sp.

ity that are similar to those of natural transcription factors and permeate live cells to localize in the nucleus in the presence or absence of any transfection agent.

2.1 Design of Sequence-Specific DNA-Binding PIP Fluorescence Conjugates. In recent years, DNA-recognition elements, such as PIPs, have been complemented with fluorescent properties. As PIP conjugates share similarity with the DBD of natural transcription factors, they may act as intrinsic probes to monitor the cellular and nuclear uptake of bioactive molecules. DNA-binding studies using PIP–fluorophore conjugates suggested their remarkable ability to induce fluorescence while maintaining a high degree of specificity and affinity after binding to their cognate DNA sequences.[18a] Interestingly, the nuclear localization of such molecules depends on a number of restrictions, such as the molecular size, pyrrole/imidazole content, and the choice of an appropriate dye.[18b] Several PIP–fluorophore conjugates display diverse photochemical properties, novel heterocycles, distinct uptake properties, bioactivity, and efficacy as anticancer compounds.[19] The excimer emission of hairpin PIP dramatically changes after the substitution of a pyrenylbutyl group. The emissions of the PIP–fluorophore conjugate excimer increase linearly with the increasing number of CAG repeats and the concentration of oligodeoxy nucleotides (ODNs) containing CAG repeats, which indicates the possibility of quantifying CAG repeat-containing DNA sequences.[20a] The evaluation of steady-state fluorescence spectra of the PIP bis-pyrenyl conjugates with rigid linkers suggested that the pyrene-functionalized PIP conjugate, which contains propynyl linkers, shows a clear increase in excimer emission that is dependent on the number of CAG repeats in the target dsDNA; moreover, the emission intensity was considerably retained (Figure 2a).[20b] Similarly, perylene–PIP conjugates were designed and synthesized using Fmoc solid-phase synthesis and a subsequent Sonogashira coupling reaction. Energy transfer from the pyrrole moiety to the perylene suggested their possible role as a molecular light switch (Figure 2b).[21] Human telomere ODNs (5′–(GGGTTA)$_4$GGG–3′/3′–(CCCAAT)$_4$CCC–5′) were detected by the combination of PIP conjugates termed **10** and **11** (Figure 2c). Excitation of conjugates **10** and **11** at 313 nm with telomere ODNs gave intense emission at 462 and 494 nm, suggesting their utility as sequence-specific fluorescence probes, because efficient heterodimer formation of a DNA-binding complex between the PIP–perylene conjugate and the telomere sequence was observed.[22] PIPs controlled the location and spatial arrangement of the fluorescent dyes within a DNA duplex at the base pair level and solved the loss of energy transfer that occurred because of inefficient self-assembly of the appropriate communicating components within DNA duplexes.[9] The design, synthesis, and evaluation of a new type of

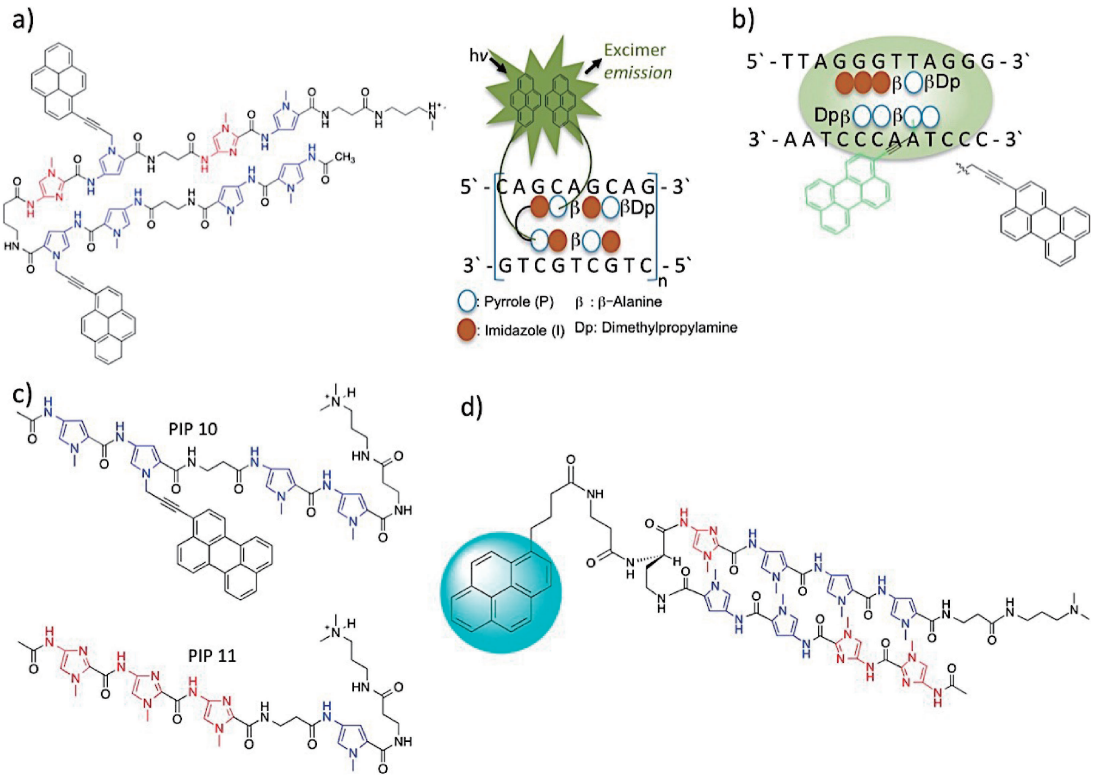

Figure 2. Design of DNA-based fluorophore conjugates. Hairpin pyrrole-imidazole polyamides (PIPs) conjugated with a) pyrene[20b] and b) perylene.[21] c) Structure of perylene–PIP fluorophore conjugates (**10** and **11**) targeting telomere ODNs (5′–$(GGGTTA)_4$GGG–3′/3′–$(CCCAAT)_4$CCC–5′).[22] d) Altered PIP–fluorophore conjugate with improved sequence specificity.[23]

hairpin PIP conjugate[23] suggested the critical role of the γ-turn position and β-alanine linker in improving sequence specificity (Figure 2d).

The efficacy of the PIP-targeting promoter of the human transforming growth factor-β1 was monitored after conjugation with fluorescein isothiocyanate (Figure 3a). The biological evaluation showed that fluorescein isothiocyanate–PIP conjugates localize to the nuclei of human vascular smooth muscle cells after 2–48 h of incubation (Figure 3b).[24a] To visualize telomeres specifically, a new synthetic route was devised to create a tandem hairpin PIP in which the tetraamide unit, which is synthesized in the solution phase, was introduced into Fmoc solid-phase peptide synthesis. The synthesized tandem PIPs were successfully targeted to human and mouse telomeres under mild conditions and allowed easier labeling of telomeres in cells, while maintaining the telomere structure. Visualization studies using the tandem PIP–fluorophore conjugates showed that the telomere length at a single telomere level is related to the abundance of the TRF1 protein, a shelterin complex component in telomeres.[24b] Characterization and microheterogeneity studies further verified the telomere staining.[24c]

To improve their selectivity to telomeres by targeting longer sequences, we designed and synthesized a fluorescent tandem trimer PIP probe that comprised three hairpins and two connecting regions (hinges). The new motif, TT59, had the ability to discriminate mismatches and recognize 18 bp dsDNA in human telomeric repeats (TTAGGG)n.[24d] The TAMRA-conjugated tandem trimer PIP probe highlighted the telomere foci clearly with lower-intensity background signals, indicating its higher selectivity to telomeres (Figures 3c and 3d). This new motif may be useful for highlighting specific regions clearly in human cells. The construction of cyanine Cy3- or Cy5-hairpin PIP conjugates and the evaluation of their binding to DNA in the nucleosome revealed the presence of a distinct binding efficacy, suggesting the possibility of characterizing the dynamic interactions within protein–DNA complexes (Figure 3e).[24e]

2.2 Gene Regulation by PIPs Mimicking Transcription Factor DBDs. PIPs targeted to a specific gene-coding region are most effective when the target sequence is unique. However, attempts to suppress gene expression using PIPs that target gene regulatory sequences were not straightforward because of the limitations of flanking sequence recognition and inhibition by nonspecific transcription factors. Targeted transcriptional inhibition by the simple binding of PIPs to specific sequences may regulate the expression of specific genes. Targeting PIPs triggered the specific regulation of the expression of therapeutically important aurora kinases (AURKA and AURKB), TGF-β1, human lectin-like oxidized low-density lipoprotein, and HER2 and EBNA1.[25] Thus, the designed PIPs successfully modulated the expression of distinct therapeutically important genes in different cell types (Figure 4a). The human ectopic viral integration site 1 (EVI1) is an oncogenic transcription factor that plays an essential role in different cancers. We have designed a PIP to target specific base pairs of the REL/ELK1 binding site in the EVI1 minimal promoter. A whole-transcriptome analysis showed that the designed PIP significantly inhibited EVI1 in MDA-MB-231 cells, as well as breast cancer cell migration.[26]

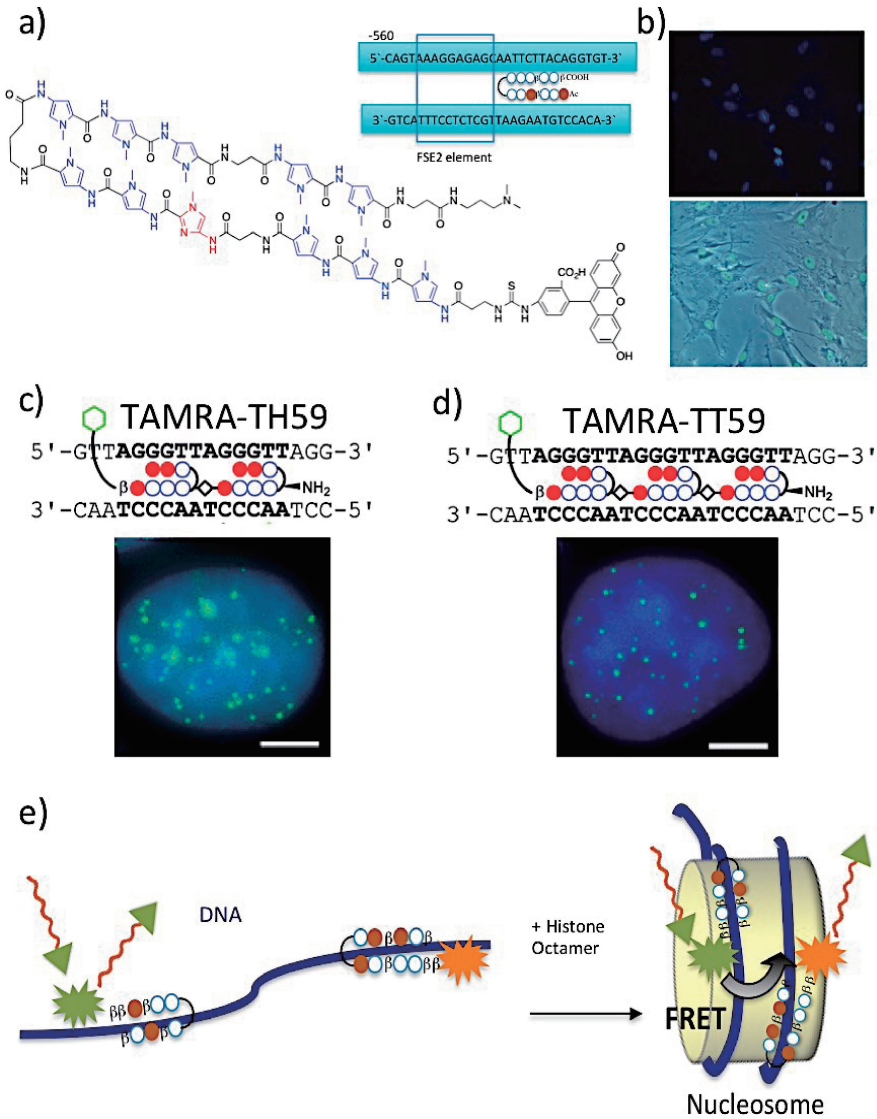

Figure 3. Bioactive PIP–fluorophore conjugates as smart fluorescent probes. a) Structure of PIP–fluorescein isothiocyanate conjugates targeting the promoter of the human transforming growth factor-β1. b) PIP–fluorescein isothiocyanate conjugates in the nuclei of human vascular smooth muscle cells after 2 h. (Figures reproduced from Lai et al.[24a]). Tandem PIP–TAMRA conjugates c) TH59 and d) TT59 targeting human telomeric repeats (Figures reproduced from Kawamoto et al.[24b,24d]). e) Schematic representation of the designed cyanine Cy3- or Cy5-hairpin PIP conjugates that facilitated the evaluation of dynamic interactions within protein–DNA complexes.[24e]

To explore the RNA-binding properties of PIPs targeting TGF-β1 and the influenza A virus (PA polyamide), we designed targeting dsRNAs and analyzed their RNA-binding properties. A Biacore assay showed the fast binding of the TGF-β1 polyamide and not the mismatch to the dsRNA. Targeting PIPs bound to RNA with a 2 log lower binding affinity compared with its DNA-binding affinity.[27] Our studies showed that PIPs can bind methylated 5′–CpG–3′ sequences.[28] Pharmacokinetic modeling studies using simultaneous urinary and biliary excretion data predicted plasma PIP concentration in rats.[29a] In addition, the pharmacokinetics of PIPs after intravenous administration in rat was reported.[29b] PIP concentration was determined in rat plasma using liquid chromatography–tandem mass spectrometry.[29c] Matrix metalloprotein 9 (MMP-9) is a therapeutically important type IV collagenase that contributes to tumor invasion and metastasis. A PIP targeting the activator protein-1 (AP-1)-binding site of the MMP-9 promoter (Figure 4b) significantly inhibited MMP-9 mRNA expression, protein levels, and enzymatic activity, as well as migration and invasion, in human breast adenocarcinoma cells (MDA-MB-231) (Figure 4c). A mouse model of liver metastasis showed decrease in liver metastasis (Figure 4d).[30] The interference of PIPs with transcriptional factors also had a positive induction effect, which suggests that PIPs inhibit both basal and activated transcription.

2.3 Alkylating PIP Conjugates as Genetic OFF Switches. The incorporation of a duocarmycin A (Du) moiety into the PIP structure improves its alkylation efficiency. The addition of distamycin A to the PIP also drastically increases DNA alkylation, primarily at the G residues of GC-rich sequences.[31] In

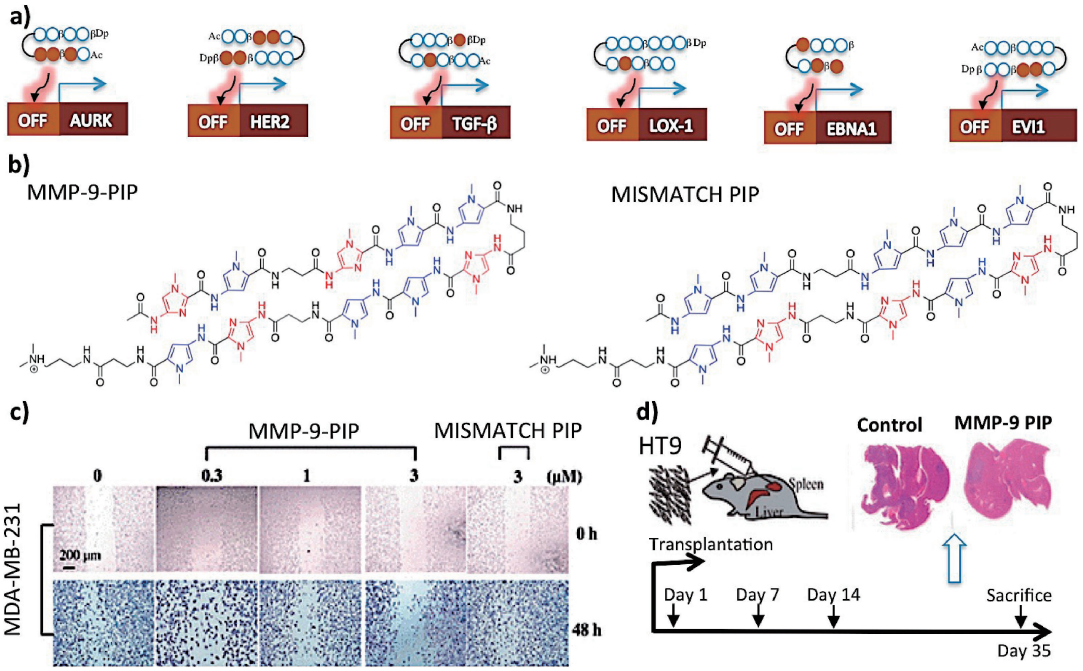

Figure 4. Gene regulation using DNA-based PIPs. a) Structure of designed PIPs that target genes in different cell types. b) Structure of match and mismatch PIPs targeting matrix metalloproteinase 9 (MMP-9), a therapeutically important type IV collagenase that contributes to tumor invasion and metastasis. c) Distinct bioactivity of match MMP-9–PIP. d) Representative mouse model studies showing the remarkable ability of MMP-9–PIP to inhibit tumor growth compared with the control (Figures reproduced from Wang et al.[30]).

our laboratory, we engineered PIPs to improve their sequence-specific efficacy and their recognition sequences by introducing vinyl linkers, L-moieties, and indole linkers.[32a] The requirement of β-alanine components in PIP conjugates with seven-base-pair recognition was shown.[32b] To extend the length of the target DNA sequence of the hairpin PIP, we designed and synthesized Y-shaped and tandem hairpin PIPs possessing 1-(chloromethyl)-5-hydroxy-1,2-dihydro-3H-benz[e]indole (*seco*-CBI) as DNA-alkylating moieties.[32c] A comparative analysis of DNA alkylation showed that PIP-*seco*-CBI conjugates were distinctly active in cells compared with PIP-chlorambucil conjugates.[32d] A long-chain hairpin PIP–chlorambucil conjugate with 11 bp recognition targeting CAG/CTG repeat sequences (which are associated with a variety of hereditary diseases) was readily synthesized via the introduction of an amino group into a GABA (γ-turn). In vitro transcription assays revealed that specific alkylation inhibited the progression of RNA polymerase at the alkylating sites.[32e]

Alkylating PIPs have been developed as anticancer agents.[33a] The cooperative alkylation of human telomere repeats by designed heterotrimeric PIP-*seco*-CBI and chlorambucil conjugates with 11 bp recognition was shown (Figure 5a).[33b,33c] The tandem hairpin motif of PIP-indole-*seco*-CBI conjugates specifically alkylated human telomere repeated sequences (Figure 5b).[33d] The design of three types of tandem hairpin PIP TH59 molecules and the evaluation of their binding efficacy revealed the presence of a small molecule with better affinity to TTAGG sequences in telomere-containing regions.[33e] One of the PIP-*seco*-CBI conjugates showed strong DNA-alkylating activity and good sequence specificity regarding the targeted histone H4 gene fragment; it also induced apoptosis efficiently in K562 cells. A genome-wide analysis further substantiated their bioactivity, as several histone H4 genes were downregulated in the presence of the PIP-*seco*-CBI conjugate (Figure 5c).[34a] The biological evaluation of two alkylating PIP conjugates with 7 bp recognition ability demonstrated their potent cytotoxicity against A549 cells and their tumor-suppressing effect on nude mice with transplantation of DU145 cells (Figure 5d).[34b]

Mutation of the *KRAS* gene frequently occurs in different types of cancer where the point mutation usually occurs at codons 12 and 13. The design, synthesis, and characterization of different types of PIP-*seco*-CBI conjugates led to the identification of a candidate with high reactivity toward the *KRAS* codon 13 mutation site, with alkylation occurring at the A of the 5′–ACGTCACCA–3′ sequence.[35a] Similarly, a PIP-*seco*-CBI conjugate that selectively recognized oncogenic codon 12 *KRAS* mutations, termed KR12, was synthesized. KR12 specifically alkylated adenine N3 at the target sequence, thus causing strand cleavage and growth suppression in human colon cancer cells carrying G12D or G12V mutations, which in turn induced senescence and apoptosis. Studies of xenograft models showed that KR12 infusions induced significant tumor-growth suppression with low host toxicity only in *KRAS*-mutated, and not wild-type, tumors. This approach could potentially be extended to target different mutant driver oncogenes.[35b] A computer-minimized model and Bind-n-Seq analysis corroborated that KR12 targets the G12D and G12V mutation sequence with much higher affinity than that observed for the wild-type sequence (Figure 5e).[35c]

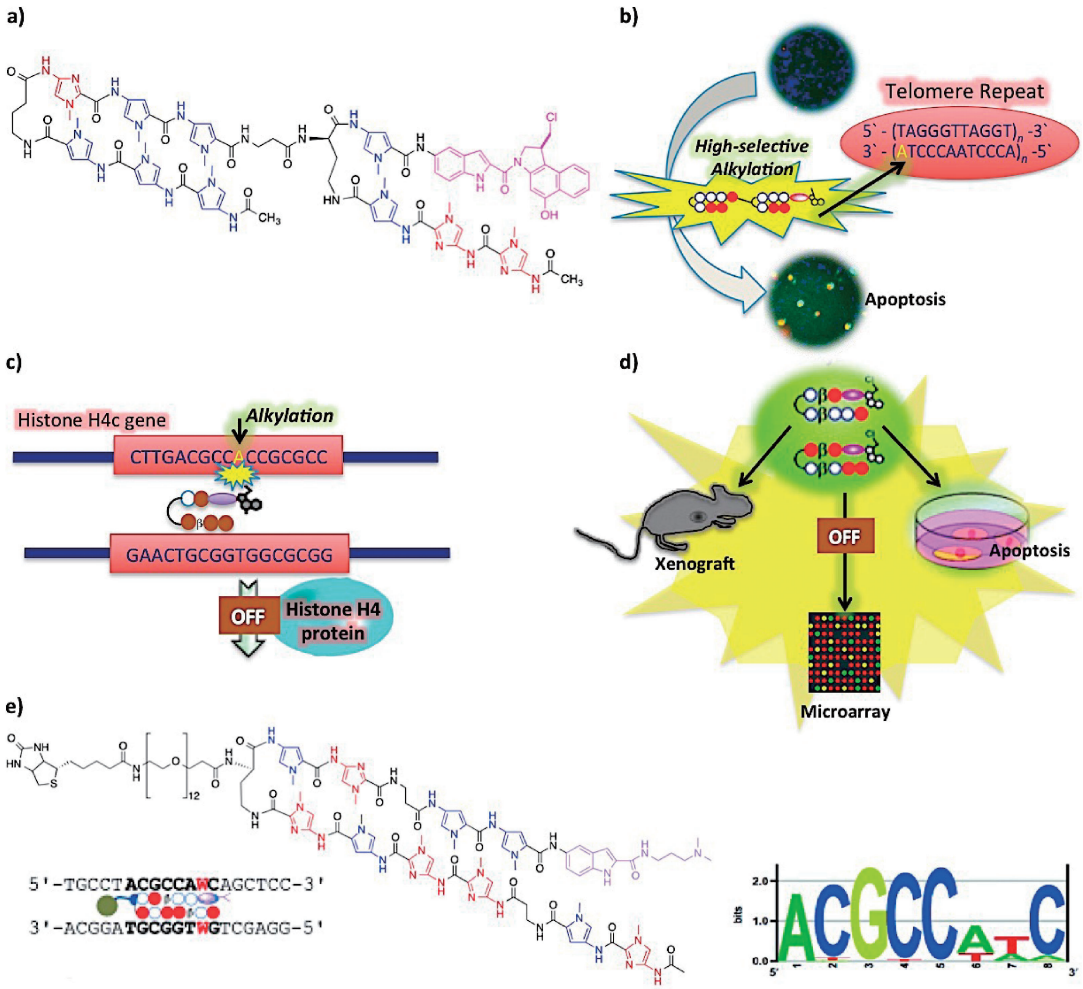

Figure 5. Development of DNA-based genetic OFF switches. a) Chemical structure of a tandem alkylating PIP.[33b,33c] b) Tandem hairpin motif of a PIP-indole-*seco*-CBI conjugate for specific alkylation of human telomere repeated sequences (Reproduced from Yamamoto et al.[33d]). c) A PIP-*seco*-CBI conjugate with strong DNA-alkylation activity and good sequence specificity regarding the targeted histone H4 gene fragment induces apoptosis efficiently in K562 cells (Reproduced from Minoshima et al.[34a]). d) Schematic illustration of two alkylating PIP conjugates with 7 bp recognition ability demonstrating their potent cytotoxicity against A549 cells and tumor-suppressing effect on nude mice with transplantation of DU145 cells (Reproduced from Kashiwazaki et al.[34b]). e) Structure of KR12 (in which the CBI unit was replaced with Dp and PEG_{12}–biotin was conjugated to the γ-turn): target *KRAS*-binding sequence and primary binding motif, as identified using Bind-n-Seq and next-generation sequencing. (Figures reproduced from Taylor et al.[35c]).

2.4 Improvement of the Chemical Architecture of PIPs. A surface plasmon resonance assay of five hairpin PIPs with a different number of imidazole rings showed that the association rate of PIPs with their target DNA decreased with the increase in the planarity of PIPs caused by imidazole.[36a] The evaluation of a single pyrrole replacement with β-alanine in a PIP targeting 5′–GCGC–3′ revealed a distinct DNA-binding affinity and increased sequence selectivity.[36b] Substitution of PIPs with a chiral β-hydroxyl-γ-aminobutyric acid/β-alanine pair effectively discriminated between T/A and A/T base pairs.[36c] Three alkylating tandem PIPs that recognize a 10 bp DNA sequence with different linkers were evaluated using high-resolution denaturing gel electrophoresis. The tandem PIP that contained a β-alanine linker displayed the most selective sequence-specific alkylation toward the target 10 bp DNA sequence.[36d] These studies provide knowledge that is fundamental to the improvement of PIP design, as small alterations in the chemical architecture of PIPs may have a notable effect on their binding efficacy. A PIP-*seco*-CBI conjugate that was protected by a photocleavable group was selectively activated by UV irradiation both in vitro and in vivo, suggesting the possibility of developing novel chemical- or enzyme-activated anticancer agents.[37a] The modification of PIP conjugates using methoxypolyethylene glycol 750 (PEG-750) improved their aqueous solubility moderately (Figure 6a).[37b] A new synthetic route to introduce a vinylpyrrole unit into the C terminus of a PIP synthesized via (fluorenylmethoxy)carbonyl solid-phase peptide synthesis and subsequent liquid-phase coupling with *seco*-CBI yielded a PIP-*seco*-CBI conjugate with a vinyl linker that recognized a 7 bp DNA sequence (Figure 6b).[37c] The conjugation of a pseudocomplementary peptide nucleic acid to a hairpin PIP selectively targeted the specific DNA sequence 5′–

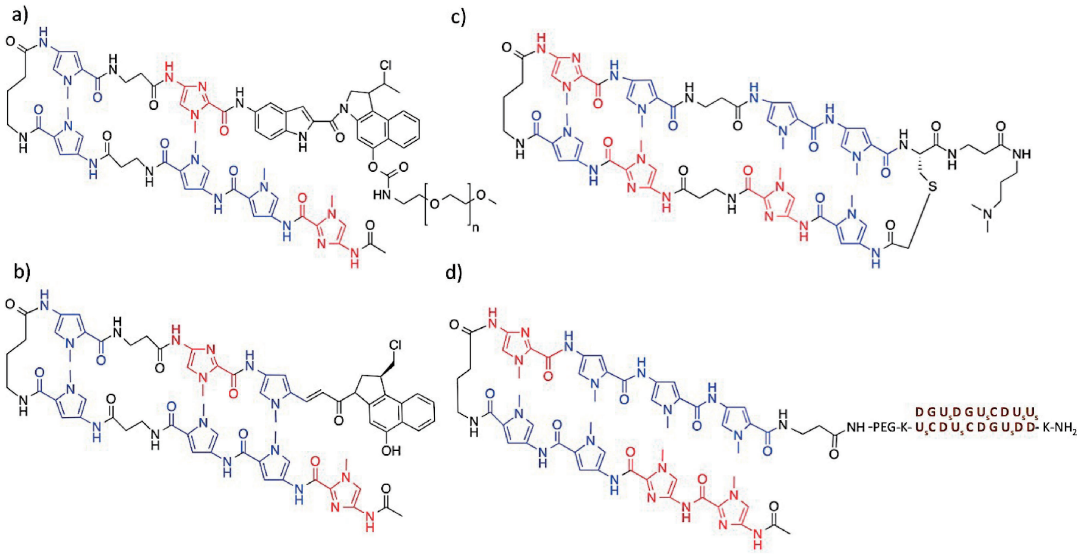

Figure 6. Chemical structure of modified PIPs and their conjugates. a) PEGylated PIP with improved aqueous solubility.[37b] b) PIP conjugates with a vinyl linker.[37c] c) Cyclic PIP with improved sequence recognition.[38a] d) Peptide nucleic acid-conjugated PIP for site-specific scission.[37d]

AGTCCT–3′ and facilitated the sequence-specific scission of long dsDNAs.[37d] A novel method that used cysteine and a chloroacetyl residue completed the cyclization reaction within 1 h and generated cyclic PIPs that recognized 7 bp DNA sequences with a high conversion efficiency. Interestingly, cyclic PIPs containing two β-alanine molecules had higher affinity and specificity than did the corresponding hairpin PIPs, which suggests the possibility of using cyclic PIPs as next-generation DNA-binding agents (Figure 6c).[38a] By extending this molecular design, an efficient cyclization reaction between a cysteine and a chloroacetyl residue was used for dimerization in the synthesis of a large dimeric PIP that recognizes a 14 bp region in duplex DNA.[38b] A pseudocomplementary peptide nucleic acid (pcPNA) is known to effectively invade dsDNA and recognize complementary A/T-rich sequences. Despite the versatile use of pcPNA in recognizing physiologically important DNA structures like G-quadruplex and telomeric DNA, their invasion efficacy was poor under physiological ionic strength conditions. We conjugated pcPNA (decamer) to a designed PIP (Figure 6d) and evaluated their efficacy. Since the binding occurred even under high salt conditions, this design overcame the technical difficulties associated with the employment of PNA-PIP conjugates in the presence of ion concentrations that is present under physiological conditions. Our chemical strategy could be successfully applied to sequence-specific DNA scission for a longer target sequence.

2.5 Design of SAHA–PIP Conjugates as Specific Genetic ON Switches. In the natural cellular environment, gene expression is orchestrated at various distinctive levels by epigenetic enzymes including histone deacetylases (HDACs) and histone acetyltransferases (HATs) that govern histone acetylation and DNA accessibility to transcription factors. Disease triggering epigenetic alteration is intrinsically flexible and can be reversed via pharmacological intervention. The inhibition of HDACs by small molecules, such as suberoylanilide hydroxamic acid (SAHA), has been harnessed to modulate gene expression. However, they operate in a sequence-independent manner.[7] In our steadfast progress to develop functional biomaterials that mimic natural transcription factors, we developed a novel class of compounds termed SAHA–PIPs that contained sequence-specific PIPs and SAHA (Figure 7a). Our designed SAHA–PIPs that targeted the promoter region of the p16 tumor suppressor gene, but not its mismatch, selectively triggered histone H3 Lys9 acetylation and induced significant morphological changes in HeLa cells.[39] Consequently, we designed 16 types of SAHA–PIPs (**A** to **P**) (Figure 7b) that were expected to yield distinct gene activation by specifically targeting a 6 bp sequence based on the binding rule of PIPs. As histone modification established and maintained pluripotency in somatic cells, these SAHA–PIPs were screened for their effect on the genes associated with the generation of induced pluripotent stem cell (iPSC) in mouse embryonic fibroblasts (MEFs). Interestingly, **D**, **E**, **J**, and **O** distinctively induced the expression of *c-Myc*, *Nanog*, *Sox2*, and *Klf4*. SAHA–PIP-mediated gene induction occurred by establishing transcriptionally permissive chromatin, including Lys9 and Lys14 acetylation and Lys4 trimethylation of histone H3.[40a] However, the induction efficiency was very low (5-fold). To improve bioefficacy, a *seco*nd library of SAHA–PIPs (**Q** to **Φ**) with improved recognition of GC-rich sequences was synthesized. Screening studies identified a potent SAHA–PIP, designated as **δ**, that was capable of inducing *OCT-3/4* and *Nanog* by about 30-fold in just 24 h and at nanomolar concentrations (Figure 7c). A microarray analysis revealed that **δ** switched ON multiple pluripotency genes by shifting the transcriptional network from the fibroblast state to the pluripotent state.[40b] Interestingly, **δ** rapidly overcame the mesenchymal–epithelial transition (MET) stage, which is an important rate-limiting step of the dedifferentiation of the somatic genome.

2.6 Genome-Wide Gene Effect of Genetic ON Switches in Human Cells. Encouraged by the bioefficacy observed in MEFs, microarray studies were carried out to evaluate the effect of 32 SAHA–PIPs (**A** to **Φ**) on genome-wide gene

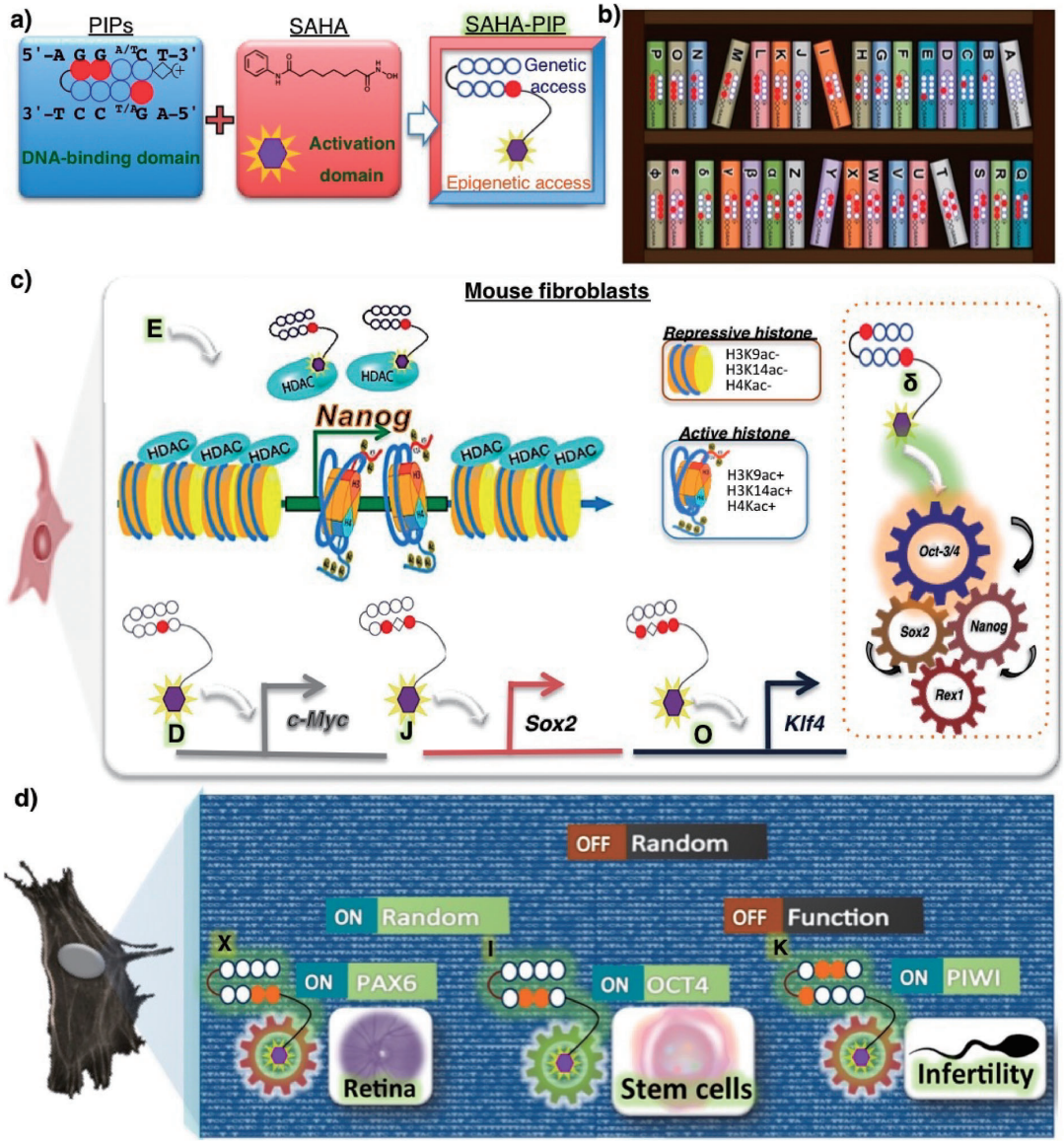

Figure 7. Synthetic DNA-based smart biomaterials with epigenetic activity. a) An innovative small molecule called SAHA–PIP capable of accessing both the genetic and epigenetic environments encompassing pyrrole-imidazole polyamides (PIPs) with the chromatin-modifying histone deacetylase inhibitor SAHA. b) Library of SAHA–PIP represented as books (**A** to **P** in the top shelf and **Q** to **Φ** in the lower shelf). c) A biological evaluation performed using mouse fibroblasts showed that SAHA–PIPs **D**, **E**, **J**, and **O** distinctively activated *c-Myc*, *Nanog*, *Sox2*, and *Klf4* via site-specific chromatin remodeling.[40a] Screening of a second library, **Q** to **Φ**, identified the SAHA–PIP, **δ**, which rapidly induced *OCT-3/4* to trigger the core pluripotency gene network.[40b] d) A genome-wide gene analysis of SAHA–PIP-treated human fibroblasts revealed that distinct SAHA–PIPs, such as **K**,[41b] **I**,[41c] and **X**,[41d] differentially activated therapeutically important retinal, stem cell, and germ cell genetic networks.

expression in human dermal fibroblasts (HDFs) (Figure 7d). Based on extensive analyses that used independent lines of evidence, we revealed the remarkable ability of unique SAHA–PIPs to trigger the transcriptional activation of exclusive clusters of developmental genes and to cause similar gene repression. Furthermore, these targeted transcriptional activators also activated a different set of noncoding RNAs and suppressed a similar set of noncoding RNAs. QRT–PCR studies validated the pattern observed in microarray analyses, that SAHA–PIPs could activate therapeutically important genes like KSR2, the obesity gene, and SEMA6A, the retinal ON circuit factor. Our proof-of-concept study suggests the possibility of modulating the transcription of therapeutically important genes and noncoding RNAs in a precise manner.[41a] A functional analysis revealed the SAHA–PIP termed **K** as the first-ever small molecule that was capable of inducing the transcriptional activation of germ cell genes in a human somatic cell.[41b] qRT–PCR studies showed that **K** remarkably induced MOV10L1, a germ-cell-specific putative RNA helicase that functions upstream of PIWI pathway factors to maintain postmeiotic genome integrity. This result is remarkable because the meiotic process is specific to germ cells and does not occur in somatic cells.

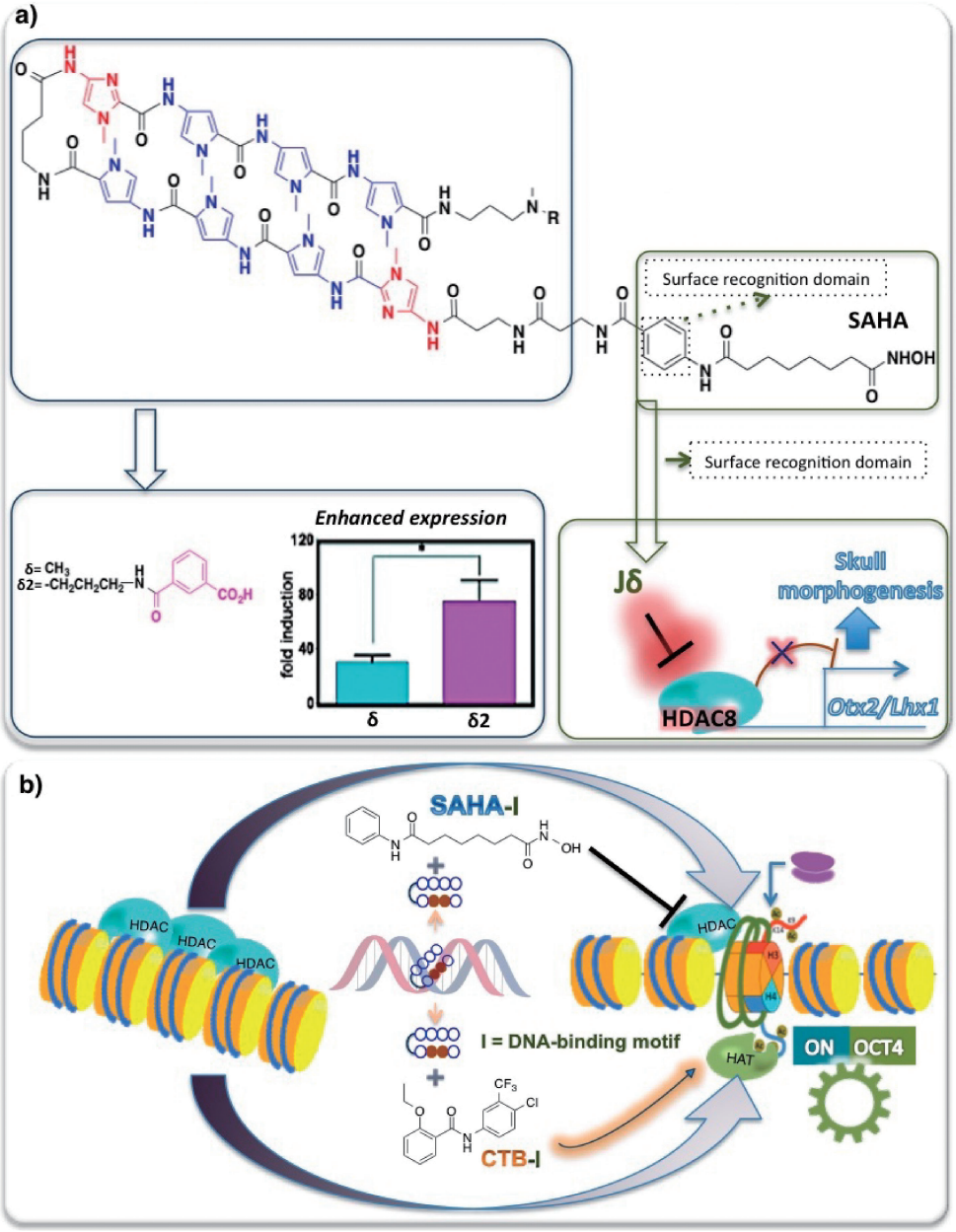

Figure 8. The alteration of smart biomaterials causes distinctive bioactivity. a) The second-generation epigenetic switch **δ2** containing isophthalic acid (IPA) at the C terminus of a PIP significantly boosted its bioefficacy compared with the unmodified **δ2**;[42c] alteration of the SAHA of SAHA–PIP generated **Jδ**, which contained specificity to HDAC8 and was active against skull morphogenesis genes, such as *Otx2* and *Lhx1*. b) The substitution of SAHA in SAHA–PIP-**I** or SAHA-**I** with the HAT activator CTB generated CTB–PIP-**I** or CTB-**I**, which remarkably activated an identical gene network governed by OCT-4 in human fibroblasts (Reproduced from Han et al.[44a]).

Interestingly, SAHA–PIP **I**, which contains a similar number of pyrrole and imidazole components as **K** but recognizes distinct DNA sequences, displayed a different bioactivity, triggered genome-wide epigenetic reprogramming, and turned ON the typically conserved *OCT-3/4* pathway genes. Moreover, SAHA–PIP **I** was identified as the first-ever small molecule that was capable of inducing the miR-302 family, suggesting the possibility of developing SAHA–PIPs as tools to activate distinctively cell-fate-regulating microRNAs.[41c] A ChIP-seq analysis and an SPR assay confirmed that SAHA–PIP **I**, but not **K**, induced hyperacetylation in the transcribed regions of *OCT-3/4*. Long-term incubation studies generated alkaline-phosphatase-positive cells with an induction efficiency of $0.06 \pm 0.03\%$ over 21 days, which suggests partial reprogramming.

Retinal tissue is part of the central nervous system and is susceptible to a wide range of disorders, such as retinitis pigmentosa (RP). A defect in the *CERK* gene, which regulates apoptosis in the retina, may result in the progression of RP. Our screening studies successfully identified a SAHA–PIP, **X**, that induced the transcriptional activation of *CERKL* and an array of potential retinal-cell-specific therapeutic genes (*PAX6*, *RS1*, *USH2A*, *CRYBB3*, and *STRA6*) that are associated with resist-

ance toward ocular disorders.[41d] A ChIP-seq analysis revealed that the highly significantly enriched motif closely resembles the potential binding site of **X** (5′–WCGGWW–3′).

2.7 Chemical Modification Aimed at Boosting the Bioefficacy of Genetic ON Switches. Modifications of the chemical architecture of genetic ON switches, such as SAHA–PIPs, are expected to improve their versatility and bioefficacy. As a first step in the evaluation of the effect of alterations in the PIP architecture of SAHA–PIPs, we synthesized different conjugates of SAHA–PIP **E** by varying the number of β-alanine linkers and the placement of the SAHA moiety. The biological evaluation of **E** conjugates that were capable of inducing *OCT-3/4* and *Nanog* expression showed that their expression levels were moderately increased in the presence of three β-alanine linkers in SAHA–PIP.[42a] We then altered the structure of SAHA in SAHA–PIP **δ** to generate a new type of small molecule called JAHA–PIP **δ** or **Jδ**, which lacked the surface-recognition domain of SAHA. An enzymatic activity assay and biological studies demonstrated that this modification could alter the HDAC specificity of **δ**, because **Jδ** displayed a significantly higher activity against HDAC8 compared with HDAC1. Interestingly, the HDAC8-specific **Jδ** also rapidly activated skull morphogenesis associated HDAC8 regulated *Otx2* and *Lhx1*, thus opening exciting opportunities in regenerative medicine.[42b] To boost the bioefficacy of **δ**, we incorporated an isophthalic acid (IPA) at the C terminus of a PIP, to improve its aqueous solubility and prevent aggregation. A biological evaluation showed that this chemical modification significantly ($P < 0.05$) boosted its bioefficacy against pluripotency genes compared with the unmodified **δ**.[42c] A next-generation sequencing (Bind-n-seq) analysis determined the sequence-specificity bias of SAHA–PIPs and led to the design of second-generation (ββ–PIPs) with enhanced binding specificity.[43] ChIP–PCR studies further showed that the model oligonucleotide duplex could be extrapolated to the corresponding sequence within chromatin. These results validate the scope of tailoring SAHA–PIPs and improving their efficacy (Figure 8a).

Transcriptionally permissive marks are acquired more reliably by activating the epigenetic writers, such as HATs, than by blocking the erasers, such as HDACs. Considering the essential role of HATs in gene regulation, we altered SAHA–PIP **I** or SAHA-**I** by substituting HDAC-inhibiting SAHA with a known HAT activator [*N*-(4-chloro-3-trifluoromethyl-phenyl)-2-ethoxy-benzamide] or CTB, to generate CTB–PIP **I** or CTB-**I**. The comparison of the bioefficacies of SAHA-**I** and CTB-**I** showed that CTB-**I** remarkably boosted the bioefficacy of CTB and activated a cluster of genes that was similar to that observed for SAHA-**I** in HDFs. An HDAC activity assay performed in cells treated with individual effectors showed that CTB did not possess HDAC inhibitory activity. A ChIP-seq analysis revealed that the peaks located around the putative promoter region were identical in CTB-**I**- and SAHA-**I**-treated HDFs. Our study suggests that distinct functional small molecules can be transformed to have identical bioactivity when conjugated with a targeting DNA-binding domain, such as PIP **I** (Figure 8b) This proof-of-concept study verified the switchable roles of HDACs and HATs in gene regulation and presented a molecular basis for the development of versatile bioactive ligands.[44a]

By conjugating CTB with a nanoparticle-based artificial transcription factor with a predesigned PIP, we successfully expanded the concept of the integration of epigenetic modulators. This platform, which was termed NanoScript, was designed to target and activate the endogenous expression of Sox9, a master regulator of chondrogenic differentiation.[44b] Fluorescence imaging and qPCR studies showed that NanoScript-*Sox9*, when incubated with adipose-derived mesenchymal stem cells, effectively activated the expression of chondrogenic markers.

3. Structural and Molecular Recognition Properties of Nucleic Acids: Mechanistic Investigation for Advancing Small Molecule Interactions

Conformational changes in DNA may influence the regulation of its biological functions, such as gene expression, in living systems. The left-handed Z-DNA represents a higher-energy form of the double helix. Sequences that favor Z-DNA formation are often located in the promoter region; hence, this type plays a critical role in facilitating transcriptional initiation and activation. The torsional strain derived from negative supercoiling, such as that generated by an actively transcribing polymerase or by a nucleosome-remodeling event, is known to stabilize Z-DNA. We demonstrated that the human SWI/SNF-complex-mediated chromatin remodeling induces Z-DNA formation on a nucleosome.[45]

3.1 G-Quadruplex Formation: Mechanism and Ligand Interaction. The G-quadruplex formation is a significant conformational change that is associated with diverse structural variations and functions. For the development of effective anticancer and anti-aging drugs, it is important to understand the functional relevance of the G-quadruplex structure in biologically significant regions, such as the single-stranded telomere terminus. In the telomere region, the association between the T-loop structure, which is suggested to protect chromosome ends, and the G-quadruplex structure is poorly understood. We proposed a model "lariat" structure in the human telomere region by designing a new, distant intrastrand quadruplex structure, and characterized its properties using CD spectroscopy, FRET, and native PAGE analysis (Figure 9a).[46a] The results of these experiments suggested that not only strand encroachment but also G-quadruplex formation stabilize the T-loop structure. The great number of tandem repeats in the human telomere may yield higher-order G-quadruplex structures; however, their orientation at the end of these structures is poorly understood. Our studies using end-extended and BrG-substituted oligonucleotides showed that the ends of stable G-quadruplex structures pointed in opposite directions and indicated that the human telomere DNA is likely to form rod-like structures (Figure 9b).[46b]

To understand the folding pathways that lead to the formation of human telomeric type-1 and type-2 G-quadruplex structures, we carried out studies using intermediate hairpin and triplex structures. Our calculation studies suggested that a triplex intermediate, as a G-triplet structure, appeared to be more stable than the hairpin conformation and was equally stable to the G-tetrad structure.[47a] The simulation studies suggested the importance of K^+ association in facilitating the overall folding via a decrease in electrostatic repulsion. Further

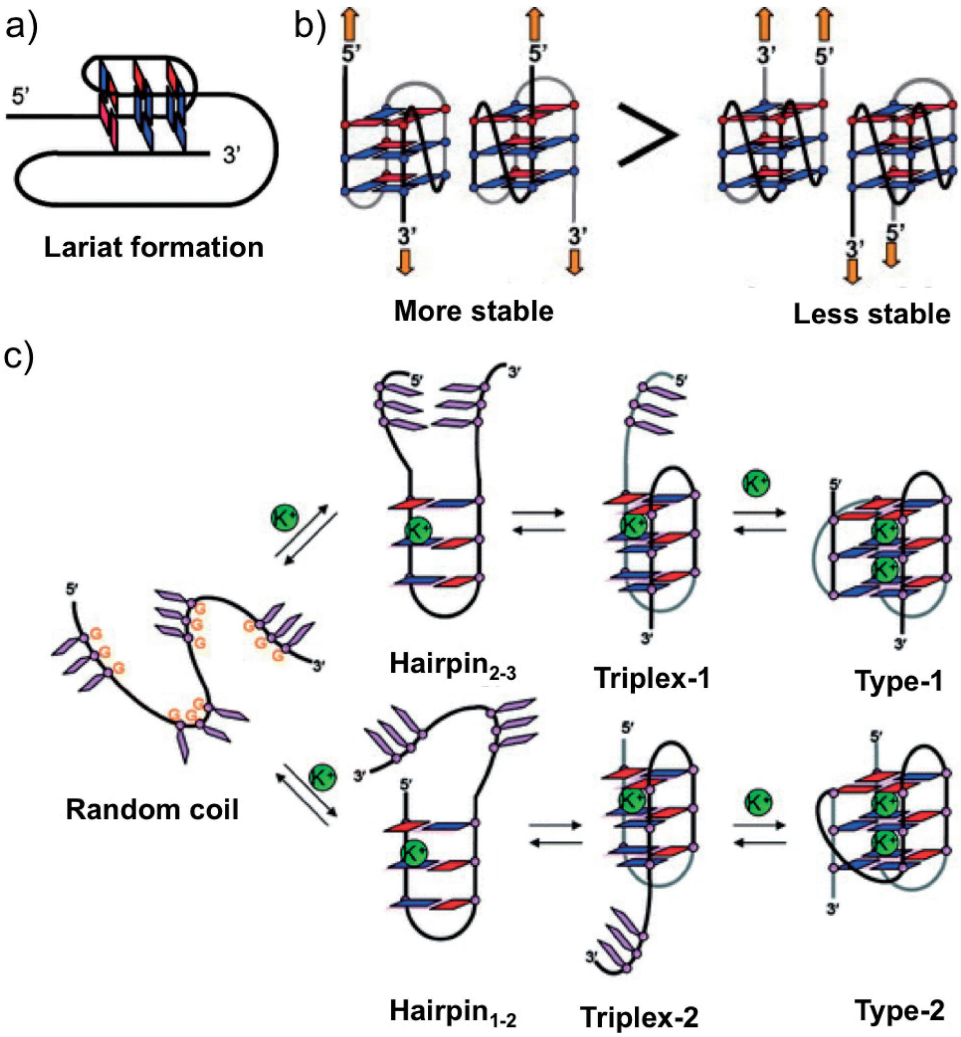

Figure 9. G-quadruplex folding pathways. a) Lariat structure encompassing a G-quadruplex and a T-loop structure (Image from Xu et al.[46a]). b) Schematic representation of the orientation of the ends of a G-quadruplex structure, as assessed using end-extended oligonucleotides (Image from Sannohe et al.[46b]). c) Folding pathways of human telomeric type-1 and type-2 G-quadruplex structures (Image from Mashimo et al.[47a]).

studies revealed the increase in the number of anti and not syn conformations with the folding and the preferential K^+ binding to a hairpin near the second lateral TTA loop. Moreover, the stacking of G-tetrads with the same conformation appeared to be more stable than the mixed equivalent. A subsequent study aimed at investigating intramolecular folding in three-tandem guanine repeats of the human telomeric DNA using optical tweezers showed the presence of a structure that was consistent with triplex conformation. Similarly, a DNA sequence with four-tandem guanine repeats showed that a similar species coexisted with a G-quadruplex (Figure 9c).[47b]

We devised an integrated approach encompassing the force-jump method and a statistical population deconvolution at the subnanometer resolution to study human telomeric sequences containing four to eight TTAGGG repeats. This fast transition kinetics study confirmed G-triplexes as the intermediates to G-quadruplexes and revealed that the long-loop G-quadruplexes were misfolded population minorities, whereas G-quadruplexes with the shortest TTA loops were the dominant species.[47c] Using the laser tweezer method, we obtained important insights into the kinetic, thermodynamic, and mechanical properties of small molecules, such as pyridostatin, that bind to telomeric DNA G-quadruplex structures.[48a] The development of small molecules that are capable of binding G-quadruplex structures is often hindered by submolecular elements, such as loops and tetraguanine planes. However, it is difficult to assess G-quadruplex stability and the roles of specific residues inside cells, and traditional studies usually involve mutations. We used click chemistry and attached pulling hands via two modified guanines in each of the three G-quartets in human telomeric G-quadruplex structures to quantify loop interaction and G-quadruplex stability at the submolecular level.[48b]

3.2 Exploiting the Photoreactivity of Nucleic Acids as a Probe. Understanding the migration of negative or positive charges (excess of electrons or electron holes) in DNA may unravel the DNA repair mechanism and be harnessed for the development of DNA-based smart nanodevices. Photoproducts that mirror the nucleic acid local structure are useful indica-

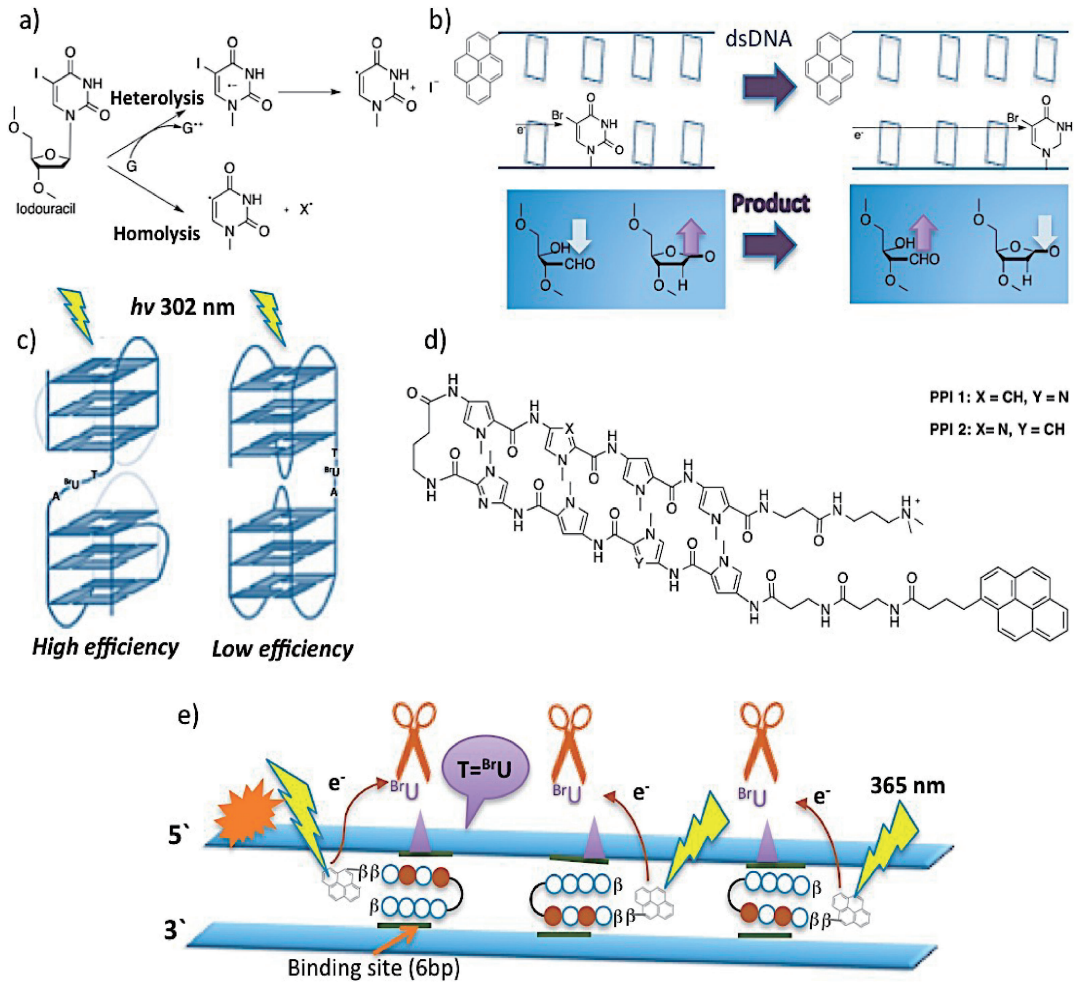

Figure 10. Photoreactivity of 5-halouracil-substituted DNA. a) Photoreaction of iodouracil in a DNA duplex showing the cleavage of a C–I bond via hemolysis and heterolysis pathways.[49b] b) A ^{Br}U-containing excess electron transfer system suggests that the distance between the donor and the acceptor affects the proportion of C1′ and C2′ oxidation products of DNA (Reproduced from Tashiro et al.[49c]). c) Photoreactivity of the linker region to two consecutive G-quadruplexes (Reproduced from Li et al.[49e]). d) Structure of pyrene-conjugated PIPs (PPIs).[51a] e) Schematic representation of the photoreaction-based detection technique that was used to screen and identify the preferential binding site of PIP (Reproduced from Saha et al.[51c]).

tors of conformational changes at sequence resolution during irradiation.[49a] To understand DNA conformational changes and reaction mechanisms that occur in a short period within a living cell, we employed photosensitive 5-halouracil-substituted DNA, in which thymine (T) was substituted with 5-halouracil moieties, such as bromouracil (^{Br}U) or iodouracil (^{I}U). The analysis of the photoreaction of iodouracil in a DNA duplex indicated that the C–I bond is cleaved via two different pathways, namely "hemolysis" and "heterolysis", and that the ratio of these pathways is dependent on the DNA sequence (Figure 10a).[49b] The efficiency of the photoinduced negative-charge transfer, termed excess electron transfer (EET), through DNA was evaluated using ^{Br}U and a naphthalene derivative as the electron donor. Despite the frequent use of ^{Br}U in a number of EET studies, the nature of the products in an EET system is poorly understood. We directly analyzed the products in an EET system using HPLC, and demonstrated that the distribution of products generated by the uracil-5-yl radical is largely dependent on the distance between the donor and the acceptor (Figure 10b).[49c] A labeling experiment using H(2)(18)O suggested the involvement of hole migration from the Py(•+) formed after charge separation in the reaction. Subsequently, we incorporated a guanosine instead of a deoxyguanosine into Z-DNA, and found that electron transfer occurred via a different mechanism, four-base π-stacks, by modifying the oxidation potential of the C2′ radical.[49d] This study contributed to the understanding of the unique four-base π-stack-based photoreactivity of Z-DNA. The photoreaction of ^{Br}U-containing DNA was used to probe two consecutive G-quadruplexes that were formed by longer human telomeric DNA. Interestingly, a notable difference in the efficiency of photoreaction was observed for eight TTAGGG repeats in K^+ and Na^+ solutions, suggesting the presence of different loop structures between two consecutive G-quadruplexes (Figure 10c). A subsequent molecular simulation generated dimeric models of the consecutive structures in K^+ and Na^+ solutions, to study and compare the loop regions located between two G-quadruplex units. Our method developed in the biologically relevant K^+ solution

potentially detected higher-order G-quadruplex formation in long human telomeric DNA in cells.[49e]

To understand RNA conformational changes, we incorporated ^{Br}U into three types of synthetic RNAs and analyzed the photoproducts using HPLC and MS analyses. In A-form RNA, the photoirradiation of r(GCA^{Br}UGC)$_2$ and r(CGAA^{Br}UUGC)/r(GCAAUUCG) yielded the corresponding 2′-keto adenosine product at the 5′-neighboring nucleotide. In Z-form RNA, the photoirradiation of r(CGCG^{Br}UGCG)/r(C^{m}GCAC^{m}GCG) yielded the 2′-keto guanosine product. Conversely, the photoirradiation of r(CGCG^{Br}UGCG)/r(C^{m}GCAC^{m}GCG) in A-form RNA yielded almost no products. Taken together, these results imply that hydrogen (H) abstraction by the photochemically generated uracil-5-yl radical selectively occurs at the C2′ position and provides a 2′-keto RNA product.[50]

The methods available currently to investigate the mechanisms of electron transfer to DNA are intramolecular. To investigate these mechanisms in an intermolecular manner, we synthesized pyrene-conjugated PIPs (PPIs) (Figure 10d) to achieve sequence-specific electron injection into DNA, and detected electron transfer using ^{Br}U as an electron acceptor. We synthesized 12 different ^{Br}U-containing oligomers and showed that the electron transfer from PPIs was localized in a range of 8 bp, thus demonstrating that PPIs can be used as a biomaterial for sequence-specific electron injection.[51a] Using slab gel sequences and a capillary sequencer, we analyzed two DNA fragments of 298 and 383 bp, respectively, to locate the uracil-5-yl radical upon 302 nm irradiation. Studies using a hydrogen donor after tetrahydrofuran and subsequent UDG treatment revealed that the employed hot-spot sequence 5′–(G/C)[A]$_{n=1,2}$^{Br}U^{Br}U–3′ and the reverse sequence 5′–^{Br}U^{Br}U[A]$_{n=1,2}$(G/C)–3′ acted in a similar fashion. This study opens the possibility of attaining information about the interface between nucleic acid and protein–DNA interactions.[51b]

A novel technique based on the photochemistry of ^{Br}U-substituted DNA was developed to detect the binding site of the gene-switching PIPs (Figure 10e). Using photoinduced electron injection, we analyzed the binding sites of four pyrene-conjugated PIPs, **1**–**4**, in two long ^{Br}U-substituted DNA fragments of 381 and 298 bp, respectively, and further estimated their binding affinity, specificity, and orientation preferences. High-resolution denaturing gel electrophoresis and PAGE analysis revealed a unique pattern: **1** and **2** injected electrons with low sequence specificity and **3** and **4** injected electrons with high sequence specificity.[51c] Interestingly, this technique also detected reverse-orientation binding sites, as observed for **2**. This platform would be useful in identifying the binding sites with the highest affinity and in facilitating the design and development of PIPs.

4. Design of Biomimetic DNA Nanostructures

DNA is a constructive molecule that is capable of achieving complicated patterns, large scaffolds, and the placement of functional molecules and nanomaterials, because of its self-assembling feature according to a predesigned program.[52] By harnessing the DNA self-assembly system, our research focuses on three broad points: (i) programmed assembly and control of nanostructures with different dimensions, and their functionalization; (ii) visualization of single-molecule interactions and chemical/enzymatic reactions in a mimicked nanospace; and (iii) construction of molecular nanosystems and nanodevices with biological applications.

4.1 Monitoring Biomolecular Interactions in Designed DNA Nanoscaffolds. Predesigned two-dimensional (2D) DNA structures facilitate the artificial reconstruction of the complicated patterns observed in the natural cellular environment to analyze single-molecule interactions and attain mechanistic insights about them. In nature, the DNA methylation enzyme *EcoR1* methyltransferase (M.*EcoR1*) bends duplex DNA to flip out the second adenine in the GAATTC sequence, thus preceding the methyl transfer reaction. To monitor this essential biomolecular interaction, we designed and prepared a rectangular 2D DNA scaffold termed "DNA frame" (80 × 90 nm) to mimic nanoscale spatial resolution and evaluate the time-resolved reaction coordination between the enzymes and the substrate. In the vacant rectangular area (40 × 40 nm) located inside the DNA frame, we introduced four connections and hybridized a tense (64mer) and a relaxed (74mer) double-strand DNA (Figure 11a). Atomic force microscopy (AFM) studies aimed at monitoring the interaction of M.*EcoR1* revealed that methylation preferentially occurred in the relaxed 74mer duplex. Biochemical analyses and RT–PCR studies further corroborated this observation, thus substantiating the critical role of structural flexibility in the methyl transfer reaction.[53a] Similarly, we artificially constructed a tension-controlled dsDNA substrate and demonstrated the significance of the bending of the duplex during the glycosylation/AP-lyation reaction of the DNA base-excision repair enzymes 8-oxoguanine glycosylase and T4 pyrimidine dimer glycosylase.[53b] To visualize the transcription process via the molecular movement of RNA polymerase (RNAP), we attached a template dsDNA (1000 bp) containing the T7 promoter at two specific positions on a DNA origami nanostructure (Figure 11b). High-speed (HS)-AFM studies showed the DNA binding, sliding, RNA synthesis, dissociation, and the mechanical behavior of RNAP during the transcription process.[53c] Moreover, we constructed a DNA scaffold to visualize the cleavage and dissociation of dsDNA by a Zn^{2+}-dependent DNAzyme, and observed the effect of configuration changes.[53d] Transcriptional regulation is influenced by the combinatorial effect of proteins. For example, the pairing of SOX2 with PAX6 triggers the transcription machinery toward a neuronal cell fate. To understand the binding mode of SOX2 to different transcription factors and their capability to swap partners, we artificially reconstructed the tensile force in the DNA frame (Figure 11c). AFM studies revealed that DNA bending is required for SOX2 binding. Moreover, the SOX2–PAX6 complex showed increased occupancy on the DNA element compared with SOX2, which validated the importance of complex formation in site-specific DNA binding.[53e]

Epigenetic enzymes, such as the Tet family proteins, convert 5-methylcytosine (mC) to 5-hydroxymethylcytosine and subsequently to 5-formylcytosine and 5-carboxylcytosine. Using an HPLC-assisted Tet activity assay, we found that CGmCGCG was a versatile substrate and demonstrated the preference of Tet toward single-stranded DNA vs double-stranded DNA.[54a] To understand the structural changes that occur in a nucleosome during epigenetic modifications, we reconstituted nucleosomes using methylcytosine- or hydroxymethylcytosine-

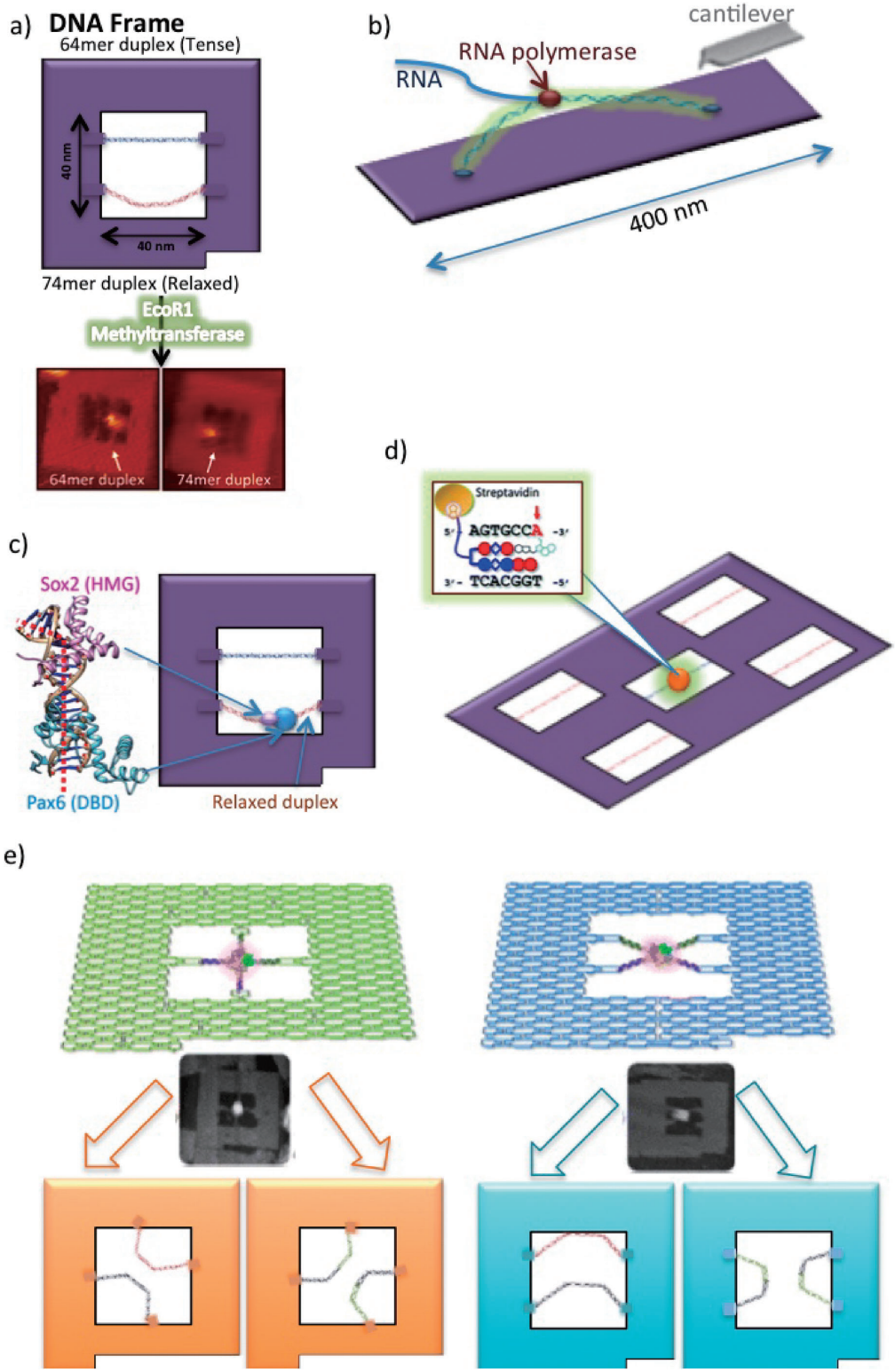

Figure 11. Visualization of protein–DNA interactions in DNA nanoscaffolds. a) Structure of a DNA nanoframe containing double strands with different tensions, to visualize the interaction of the DNA methylation enzyme *EcoR1* methyltransferase (M.*EcoR1*) (Reproduced from Endo et al.[53a]). b) A defined DNA nanostructure that was used to visualize the transcription process via the molecular movement of RNA polymerase (RNAP) in a template dsDNA (1000 bp) containing the T7 promoter (Reproduced from Endo et al.[53c]). c) DNA origami frame used to visualize *Sox2*–Pax6 complex formation on a regulatory DNA element (Reproduced from Yamamoto et al.[53e]). d) A five-well DNA nanoscaffold used to visualize the sequence-specific single-molecule alkylation of PIP (Reproduced from Yoshidome et al.[55a]). e) Visualization system used for studying site-specific recombination events (Reproduced from Suzuki et al.[56a]).

substituted DNA. AFM studies showed that cytosine methylation induced a larger effect on the overwrapping of the DNA around the histone octamer compared with that observed for cytosine hydroxymethylation. This observation suggests that different DNA modifications influence the compaction and relaxation of the chromatin structure, which in turn regulate gene expression.[54b]

Synthetic alkylating PIPs modulate selective gene transcription via the sequence-specific alkylation of target dsDNAs. To directly visualize the selective alkylation of the target site by alkylating PIPs, we designed a new DNA scaffold termed "five-well DNA frame" that contained five different dsDNA sequences (Figure 11d). Visualization studies using a doubly functionalized PIP with *seco*-CBI and biotin showed the alkylation of the fully-matched target sequence AGTXCCA/TGGYACT (X = G) with 88% selectivity; moreover, they effectively discriminated one-base mismatched (X = A, T, C) sequences.[55a] This observation validated the selective alkylating efficacy of PIP conjugates. Similarly, the site-specific positioning of the selective gene that modulates zinc finger proteins (ZFPs) was shown on DNA origami structures, thus substantiating the distinct recognition ability of ZFPs.[55b] Site-specific recombination is a form of genetic recombination that involves the reciprocal exchange between defined DNA sites. The actual role of the topological state of the substrate in the formation of a recombinase–DNA synaptic complex remains unknown. For this purpose, we reconstructed this event in a DNA-frame nanoscaffold. HS-AFM analyses revealed that the loxP-containing substrate strands in the antiparallel orientation recombined only via the formation of synaptic complexes (Figure 11e). DNA frames tethered with Holliday junction (HJ) intermediates as a starting substrate in different connection patterns suggested that the topological state of the HJ intermediates dictates the outcome of the resolution.[56a]

As HJ resolution is a critical step in the completion of homologous recombination, we reconstructed flexible and inflexible junctions and found that only flexible junctions were efficiently resolved into two duplexes upon binding to *Bacillus subtilis* RecU HJ resolvase. This study demonstrated the significance of structural malleability and cleavage preferences in this process.[56b] To directly visualize the DNA structural changes that occur upon photosensitization, we introduced a pair of photoresponsive oligonucleotides containing azobenzene moieties into the double-stranded DNA within the DNA frame. AFM studies clearly demonstrated that the two dsDNAs were dissociated by UV irradiation and hybridized under visible light, which suggests the establishment of an observation system for investigating molecular switches at the single-molecule level.[57a] RNA molecules underwent structural changes via specific hairpin loops to form a complex termed "kissing complex". To study the interaction between RNA molecules and molecular switches, we introduced two types of RNA molecules into a DNA origami structure and studied their interaction with ligands at the single-molecule level. AFM studies demonstrated the switching function of a designed RNA aptamer called guanosine triphosphate (GTP) switch that can bind to the target RNA hairpin in the presence of GTP in the nanospace.[57b]

4.2 Monitoring DNA Conformational Changes in Designed DNA Nanoscaffolds. The visualization of DNA conformational changes in a defined nanoscaffold may facilitate the wider understanding of structural changes and reaction mechanisms. A defined nanosystem that was constructed to control the binding of the Zαβ protein to the target sequence showed that the rotation of the double helix is a critical factor for protein binding and reactions. We characterized the properties of Zαβ binding to the analogues of a (CG) repeat sequence and demonstrated its preferential binding to the Z-form.[58a] We mimicked rotary proteins by constructing a DNA-based molecular machine with rotary function, and visualized the B–Z conformational transition within a DNA frame. We switched the motor ON and OFF by introducing conditions that stabilize B-DNA and by adding a Z-DNA-promoting high-saline buffer, respectively.[58b] External stimulation with $MgCl_2$ rotated 70% of the motors, but not the stators/controls (Figure 12a).

In 2010, we used HS-AFM to report the first-ever real-time observation of a reversible DNA conformational change by monitoring the G-quadruplex-induced global change of two duplexes incorporated into a DNA nanoscaffold.[59a] The introduced G-rich strands formed an interstrand (3+1) X-shaped state via the addition of K^+, whereas the removal of K^+ disrupted the structure, to create a parallel state (Figure 12b). We successfully performed a two-step cascading transformation reaction in a single DNA nanosystem by integrating a wavelength-dependent photoswitch and a metal ion-dependent switch (K^+).[59b] Using HS-AFM, we observed a series of dual-switching logical behaviors that corresponded to conformational changes (Figure 12c). This system may contribute to the tracing of signal conversion in DNA computing and to creating versatile sensing devices. We developed a nanosystem to demonstrate the formation and dissociation of dsDNAs containing the GQ sequence and the counterpart i-motif sequence at the single-molecule level (Figure 12d). The topologically controlled GQ/i-motif dsDNA in the DNA frame was obtained in high yield via sequential manipulation of DNA strands, the toehold strand, and the addition and removal of K^+. The GQ/i-motif duplex prepared in this way resolved the dsDNA into the GQ sequence and the i-motif by the addition of K^+ and/or under an acidic condition in the promoter region. The dissociation of a dsDNA containing the GQ- and the i-motif-forming sequence was monitored and controlled in the DNA frame. This system is useful to elucidate the dynamic formation of the GQ and i-motif involved in the regulation of gene expression in the promoter region.[59c]

We incorporated two duplex DNAs inside a DNA origami frame with G–G mismatch repeats in the middle of it, to monitor the topological changes of the strands.[60a] The addition of KCl induced DNA synapsis without disturbing the duplex regions of the participating sequences and resulted in an X-shaped structure. This arrangement allowed control of strand orientation and topology and of the stoichiometry of G-quadruplex formation. Subsequently, we performed a real-time analysis of the chaperone activity of HIV-1 nucleocapsid proteins (NCps), which facilitate the remodeling of nucleic acids during G-quadruplex formation.[60b] The analysis of the properties of the proteolytic intermediate NCp15 and the mature NCp7 revealed that the protein particles primarily existed in monomeric form and provided stoichiometry data regarding the formation and

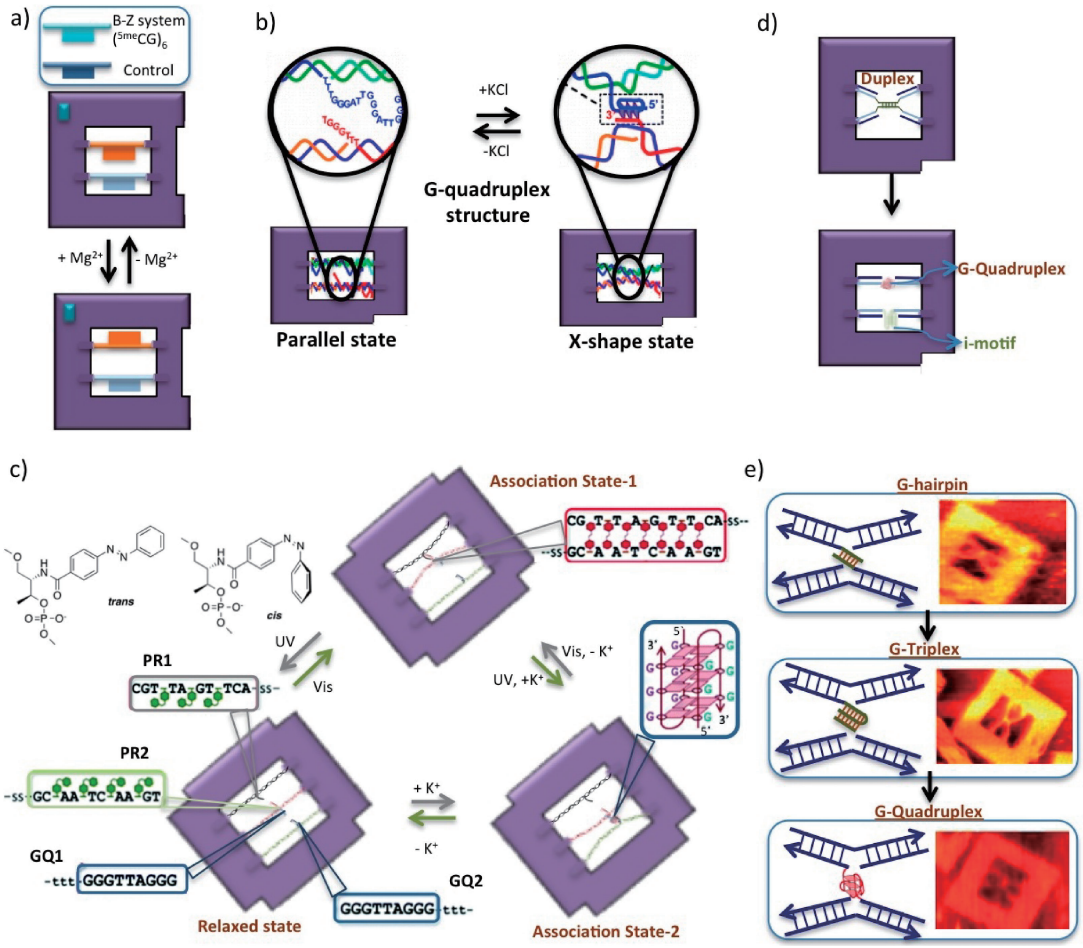

Figure 12. Visualization of DNA conformational changes. a) A rotary protein mimicking a DNA-based molecular machine with rotary function was used to visualize the B–Z conformational transition (Reproduced from Rajendran et al.[58b]). b) DNA-based nanosystem used to visualize the reversible G-quadruplex conformational transformation (Reproduced from Sannohe et al.[59a]). Schematic illustration of the monitoring of c) dual-switching behaviors corresponding to the state transition in a DNA nanoframe (Reproduced from Yang et al.[59b]) and d) the single-molecule manipulation of duplex formation and dissociation at the G-quadruplex/i-motif site (Reproduced from Endo et al.[59c]). e) Single-molecule visualization of the solution-state structures of G-hairpin and G-triplex intermediates (Reproduced from Rajendran et al.[61b]).

dissociation events. This study may contribute to the design of anti-HIV drugs based on G-quadruplexes. The G-quadruplex-binding ligands may be used to target the G-rich sequences that occur in human chromosome telomeres and in the promoter region of several proto-oncogenes. We visualized directly the formation of a G-quadruplex structure using bisquinolinium pyridine dicarboxamide with a linker containing biotin at one end.[60c]

This system facilitated the nanoprecise capture of unprecedented solution-state structures of a tetramolecular antiparallel and of (3+1)-type G-quadruplex intermediates (Figure 12e).[61a] The stable intermediates, such as G-hairpins and G-triplexes, formed with good yield. Moreover, the interplay between these intermediates, divalent Mg^{2+} ions, and monovalent K^+ ions was shown. These results substantiated our previous simulation study of G-quadruplex folding pathways.[47a] Consequently, we also captured the solution-state structures of the complexes that were formed between streptavidin and a G-hairpin/G-triplex and revealed that the binding of ligands to the intermediates leads to stepwise folding into a quadruplex structure.[61b] The development of this system may provide a broader understanding of the interaction between G-quadruplexes and their targeting drugs.

4.3 Programmed Assembly of Nanostructures with Different Dimensions. The programmed assembly/control of nanostructures with different dimensions is among the ultimate goals of supramolecular chemistry and is a critical method in bottom-up nanotechnology. Rothemund et al. reported that DNA origami, a DNA self-assembly system, can be used to construct fully addressable 2D plates and different 2D structural patterns. The combination of the DNA origami method for the preparation of 2D DNA scaffolds and subsequent folding via their connection strands allowed us to achieve three-arm (Y-shaped), four-arm (X-shaped), and six-arm (asterisk-shaped) structures. Using a template single-stranded DNA (M13mp18), nine strands were introduced into one side of each arm, to connect to the adjacent arm. Two thymidines (T2) were introduced to connect a counterpart site on the adjacent arm, for flexibility during the hybridization of the connection strands. The designed hollow three-dimensional (3D) prism structures com-

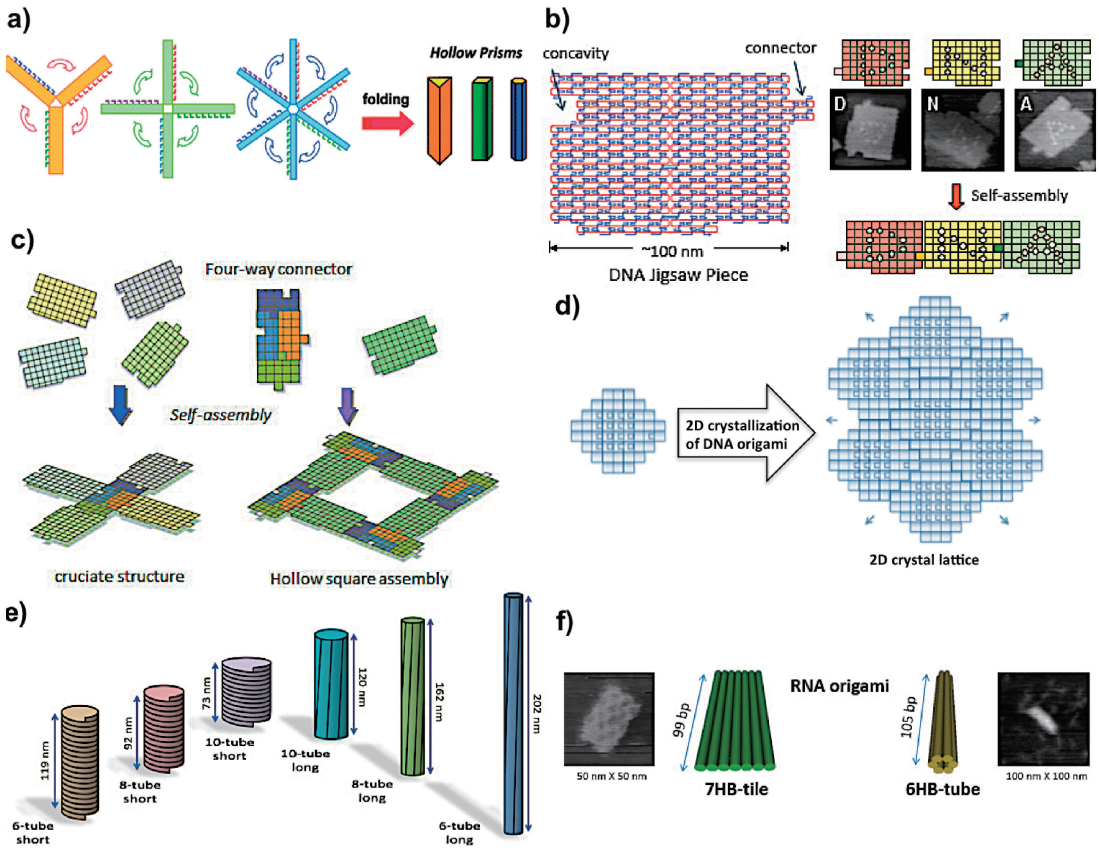

Figure 13. Programmed assembly of nanostructures. a) Multiarm DNA structures with connection strands that were folded to produce hollow prism structures (Image from et al.[62]). b) Designed 2D DNA origami rectangles with sequence-programmed connectors formed "DNA jigsaw pieces" (Image from Endo et al.[63a]). c) A four-way connector with connection sites at all four edges was assembled to form a cruciate and a hollow square structure (Image from Endo et al.[63b]). d) Illustration of the 2D crystallization of DNA origami with different loop arrangements (Image from Rajendran et al.[63d]). e) Helical DNA origami tubular structures with various sizes and arrangements (Image from Endo et al.[64b]). f) Schematic of the preparation of chemically modified RNA origami nanostructures Helical DNA origami tubular structures with various sizes and arrangements (Image from Endo et al.[64c]).

prised three (eight helices), four (six helices), and six (four helices) rigid rectangles (24 helices) and were connected by flexible hinges (Figure 13a).[62] We developed a novel method to design 2D DNA origami rectangles, termed "DNA jigsaw pieces," and contained sequence-programmed connectors. For the selective connection of DNA rectangles, we introduced shape and sequence complementarity into the concave and convex connectors via nonselective π-stacking interactions between the side edges of the DNA jigsaw piece structures. We assembled three and five DNA jigsaw pieces with the correct alignment and uniform orientation into predesigned ordered nanostructures, to obtain three-, four-, and five-letter words (Figure 13b).[63a] Subsequently, a four-way connector led to the successful assembly of five and eight origami monomers and the formation of a cruciate and a hollow square structure, respectively (Figure 13c).[63b] We scaled up the origami structures to achieve the programmed 2D self-assembly of multiple DNA origami jigsaw pieces. To accomplish 2D self-assembly along the helical axis (or horizontal direction) and the helical side (or vertical direction), we introduced a sequence-programmed structure (tenon and mortise) and the sequence complementarity of single-stranded overhangs, respectively. The design and preparation of nine different jigsaw pieces to attain a 3 × 3 assembly in four different ways showed that the stepwise self-assembly from the three vertical trimer assemblies gave the intended 2D construction with a yield of about 35%. The surfaces of the jigsaw pieces decorated with hairpin DNAs self-assembled into a 2D structure and displayed letters that formed the word "DNA JIG SAW" at the nanoscale.[63c] To achieve control over the 2D crystallization of DNA origami, we introduced loops on their surface. Studies performed using different orientations revealed that the vertical alignment was the only appropriate orientation to attain the 2D crystal lattice on a micrometer scale (Figure 13d).[63d]

The controlled assembly of the kinetic and thermodynamically stable G-quadruplex DNA structure is difficult because of the rules of recognition. To overcome this issue, a design was proposed that combines parallel-stranded duplexes and a quadruplex core, to assemble and visualize quadruplex-based 1D structures that are capable of accommodating potential modifiers.[64a] The DNA origami method was used to design and prepare the size-controlled tubular structures 6-tube, 8-tube, and 10-tube, which contain 192, 256, and 320 base pairs over one round, respectively (Figure 13e).[64b] A detailed analysis of the tube surface patterns showed that the expected short tubes and unexpected long tubes had mainly a left-handed helical

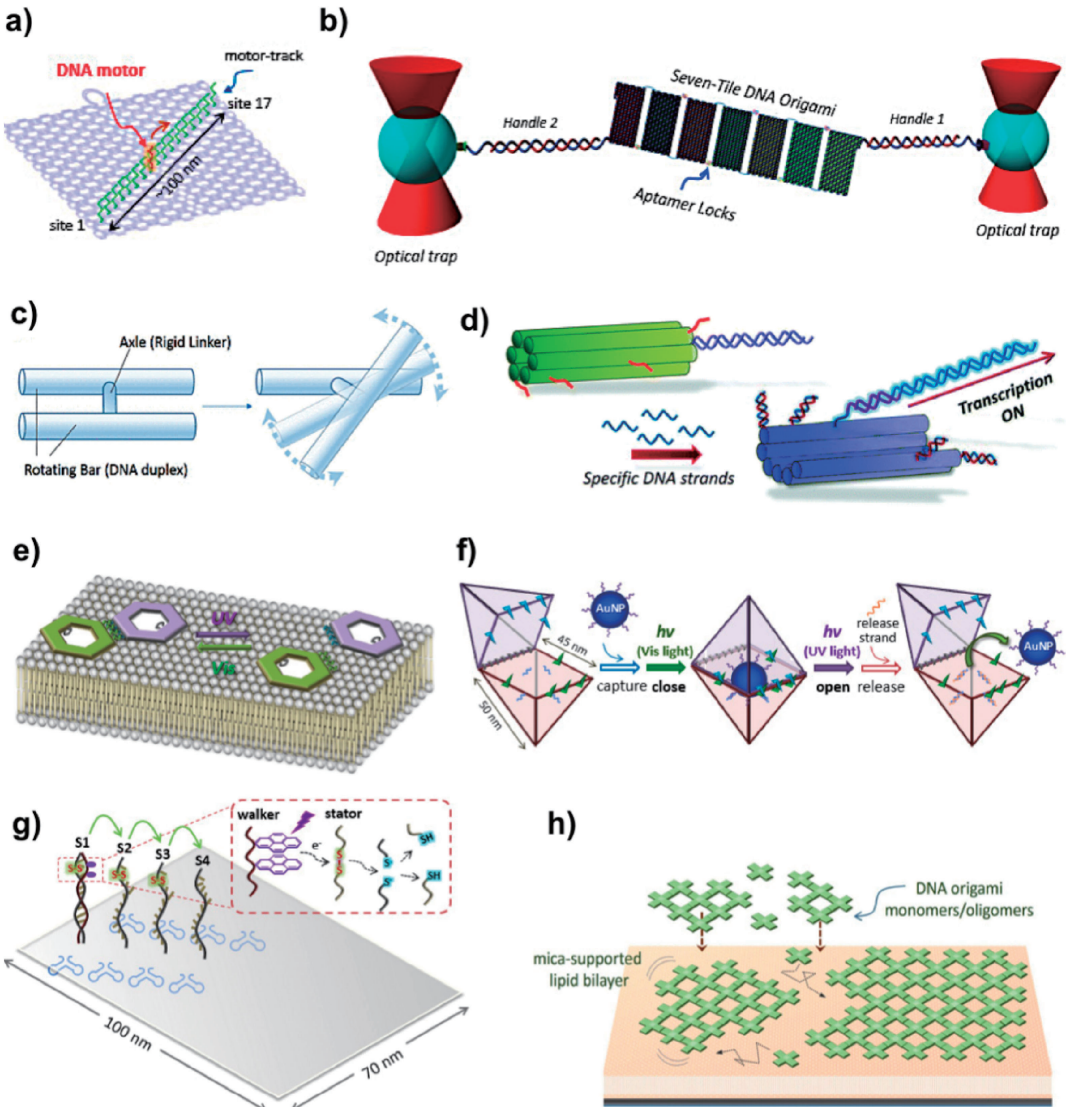

Figure 14. Guided assembly of nanostructures. a) A DNA transportation system constructed using a mobile DNA nanomachine along a designed track on the DNA origami surface (Image from Wickham et al.[65a]). b) A single-molecule mechanochemical sensing platform with a seven-tile DNA origami nanostructure (Image from Koirala et al.[66b]). c) Simplified illustration of the molecular model of a novel rotatable DNA unit (Image from Tashiro et al.[66c]). d) Schematic representation of a transcription-regulation system mediated by the mechanical operation of a DNA nanostructure (Image from Endo et al.[66d]). e) Dynamic assembly/disassembly of photoresponsive DNA origami nanostructures visualized on a lipid-bilayer membrane surface (Image from Suzuki et al.[67c]). f) Photoresponsive DNA nanocapsule with an open/close system for the capture and release of nanomaterials (Image from Takenaka et al.[67d]). g) A photocontrolled DNA nanomachine on the DNA nanostructure (Image from Yang et al.[67e]). h) Lipid-bilayer-assisted 2D self-assembly of DNA origami nanostructures (Image from Suzuki et al.[70]).

structure and right-handed structure, respectively. Interestingly, the population of the left-/right-handed and short/long tubes changed in accordance with the number of base pairs involved in one round of the tubes. The variable formation of tubular structures is suggested to be associated with the helical stress caused by the stiffness of the double helices and the nonnatural helical pitch in the DNA origami design. Using RNA templates containing chemically modified uracils, we constructed RNA-templated DNA origami structures by annealing with designed DNA staple strands and folding, to form seven-helix bundled rectangular structures and six-helix bundled tubular structures (Figure 13f).[64c] We successfully used cationic comb-type copolymers as locks based on their ability to restrict origami folding by binding to the phosphate backbone of M13mp18/staples, together or alone. We used polyvinyl sulphonic acid as a key to demonstrate the controllable fabrication of DNA origami structures.[64d]

We constructed a cuboid structure based on a square prism structure and characterized the structure using AFM and dynamic light scattering.[64e] This study proposes the development of functional nanostructures with controllable closing and opening processes.

4.4 Guided Assembly and Control of Molecular Nanosystems and Nanodevices. Molecular assembly assisted by factors such as enzymes and light may guide the design and control of molecular nanosystems and nanodevices. Using

Watson–Crick base pairing, a molecular transportation system was constructed in which the track, a motor, and fuel were all prepared from DNA. The DNA nanomachine system was loaded at one end of the track and moved autonomously along the full length of the track that was designed to contain 17 stators on the DNA origami scaffold using 16 consecutive steps (Figure 14a). Visualization studies using AFM suggested that this stepwise-controlled movement is one directional and time dependent, which indicates the potential use of this system to create molecular assembly lines modeled on the ribosome.[65a] Similarly, a branched motor track with three branching points and four final destinations was constructed on the DNA origami scaffold. The pathway and destinations of the DNA motor were controlled in a programmed fashion using the block strands at both sides of the branching points and the corresponding release strands. The navigation of the DNA to the final destination was observed using AFM and the fluorescence quenching method.[65b]

We also developed a novel DNA scaffold, called a DNA slit, for the thiol-guided programmed placement of Au nanoparticles.[66a] A DNA origami method based on mechanochemical principles was developed to construct a throughput single-molecule biosensing platform by incorporating six sensing probes at different locations of a seven-tile DNA origami template (Figure 14b). The probes used in this platform induce the rearrangement of the 2D or 3D origami nanostructure upon binding of a target molecule and can be monitored in real time using optical tweezers. This proof-of-concept study demonstrates the ability of this platform to detect the platelet-derived growth factor at 10 pM and to differentiate it from a DNA target in a multiplexing fashion.[66b] The development of a versatile DNA origami nanoassembly is expected to overcome the restriction of sensing events that are carried out one at a time and offers a much-needed solution for high-throughput sensing at the single-molecule level. A novel chemically modified H-shaped DNA oligonucleotide was designed and synthesized via cross-linking with a structurally rigid linker consisting of phenylene and ethynylene groups, to construct a rotatable DNA unit with two complementary DNA oligonucleotides. This novel rotatory DNA unit may serve as an effective component of large DNA machines (Figure 14c).[66c] We designed and constructed a transcription-regulation platform in which specific DNA strands induced the opening of the six-helix bundled tubular structure using the toehold system (Figure 14d). The addition of specific DNA strands successfully released a transcription product from the purified tube-attached dsDNA template, which suggests the use of a nanostructure that is capable of acquiring vital mechanistic information.[66d]

The photo-cross-linking of 8-methoxypsoralen improved the thermal stability of DNA origami structures. This temperature-assisted cross-linking was used to assemble and disassemble origami at higher and lower temperatures, respectively.[67a] The introduction of photoresponsive DNAs into hexagonal DNA origami structures yielded exclusive patterns of multidirectional-programmed 2D DNA nanostructures via irradiation at different wavelengths in a programmed manner. Alterations of the number and position of photoresponsive DNAs in the hexagonal units produced specific face-controlling nanostructures that facilitated the construction of curved and ring-shaped nanostructures.[67b] We introduced cholesterol moieties into the hexagonal origami structures; the outer edges of one of these structures carries Azo-ODNs. This assembled bilayer-placed hexagonal dimer was disassembled into monomer units and reversibly reassembled under UV irradiation and visible-light irradiation, respectively. These dynamic assembly/disassembly processes were directly visualized using HS-AFM (Figure 14e).[67c] A square bipyramidal DNA nanocapsule (NC) with a photocontrollable open/close system and a toehold system was designed as a nanomaterial carrier. The hybridization of a specific DNA (capture strand) facilitated the encapsulation of the DNA-modified gold nanoparticle (AuNP) into the NC. The addition of a toehold-containing complementary DNA (release strand) successfully released the AuNP from the NC (Figure 14f).[67d] We devised a light-driven artificial molecular nanomachine with the aim of introducing cargo transport and manual configuration alterations in mesoscopic systems. A walker–stator duplex was designed in which the walker (i.e., a single-stranded DNA that carried two pyrene molecules) was located on the surface of the DNA tile, which was assembled using a 2D DNA tile that carried four stator strands as the linear track. Via the excitation of the pyrene molecules ($\lambda_{ex} = 350$ nm), the walker induced the cleavage of disulfide bonds in stator strands and initiated the continuous migration of the DNA walker from one cleaved stator to the next intact stator, until it reached the final stator. The light-fuelled movements of this light-driven nanomachine were directly observed in real time under UV irradiation using HS-AFM (Figure 14g).[67e]

We designed and developed different kinds of DNA assemblies with polypod-like and Takumi-shaped structures as effective nanovehicles for the delivery of immunomodulating nucleic acids to immune cells.[68] RNA–protein complexes with different shapes were engineered for imaging and therapeutic applications.[69] We constructed "lipid-bilayer-assisted self-assembly" structures in which DNA origami nanostructures assembled into 2D lattices. We used mica-supported zwitterionic lipid bilayers to absorb DNA origami structures electrostatically in the presence of divalent cations. These origami units are mobile on the surface and can self-assemble into large lattices (with a μm size in lateral dimensions) (Figure 14h). HS-AFM revealed the dynamic processes, such as growth and reorganization, of lattices. The in situ decoration of the assembled lattices hinted at the scope of surface modification. This new strategy represents a significant advancement in the design and fabrication of novel supermolecular architectures and in the organization of functional nanodevices (in μm space).[70] In addition, we were able to mimic the dynamic assembly of membrane-associated protein clusters that play an essential role in the formation of cellular membranes.

5. DNA-Based Systems for Practical Applications

5.1 Design of DNA-Based Switching Devices. Because topologically interesting molecular architectures, such as catenanes, display unique physical properties, strategies aimed at constructing such architectures are of great interest. We developed a novel strategy to synthesize a heat-resistant DNA catenane using the formation of a G-quadruplex structure via the cyclization of DNA through the covalent bond connec-

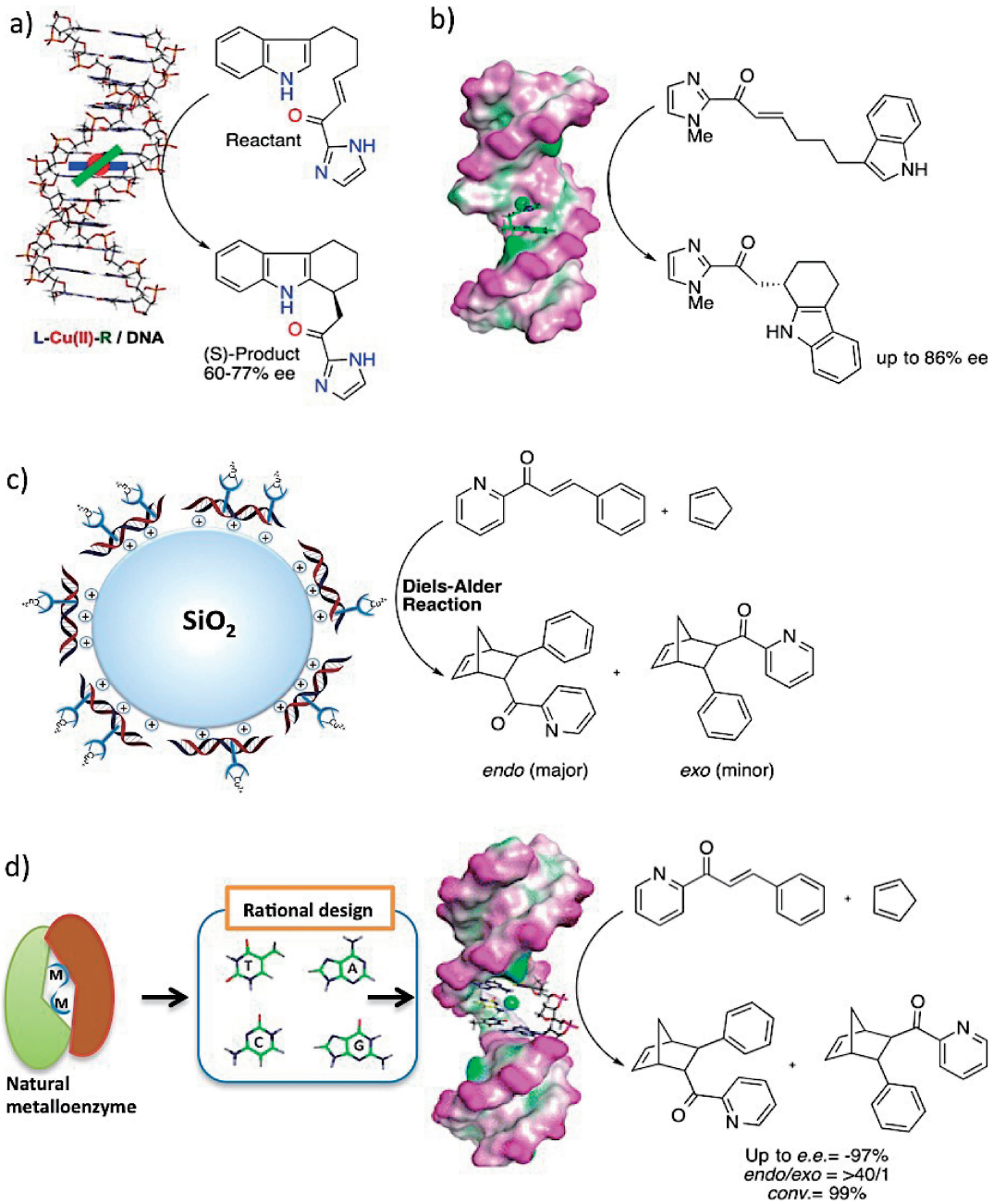

Figure 15. DNA-based hybrid catalyst. Illustration of a) L-Cu(II)-R/DNA catalyzed unimolecular Friedel–Crafts reaction (Reproduced from Petrova et al.[73b]). b) DNA-based hybrid catalyst with an intramolecular ligand (Reproduced from Park et al.[73c]). c) Solid-supported DNA used for asymmetric synthesis (Reproduced from Park et al.[74a]). d) Rational design approach for the development of nature-inspired DNA metalloenzymes that are capable of catalyzing asymmetric Diels–Alder reactions (Reproduced from Park et al.[74b]).

tion.[71] To advance the application of long fluorescent DNAs, we synthesized a highly emissive thioanalogue of **thdGTP** and enzymatically incorporated it into DNA via primer extension and PCR amplification. The synthesized 2-aminothieno[3,4-d]-pyrimidine G-mimic deoxyribonucleoside (**thdG**)-labeled DNA was amplified by natural polymerases and **thdGTP** was added to the standard PCR mix in a straightforward manner.[72a]

Subsequently, we incorporated **thdG** readily into oligonucleotides and demonstrated that Z-DNA was successfully detected based on the different π-stacking properties of B- and Z-DNA.[72b] As an analogue of **thdG**, 2′-OMe-**thdG**, effectively induced Z-form DNA, we constructed a visible nanothermometer based on the B–Z transition of DNA.[72c] We synthesized various oligomers of $d(CG)_n$ or $d(GC)_n$ containing 8-methylguanine at a different position. CD spectra studies showed that the order of arrangement of m(8)G and m(8)rG in DNA strands influenced the Z-DNA stabilizing effect and that the center position effectively stabilized and promoted the B–Z transition.[72d]

5.2 Development of DNA as a Catalyst for Organic Synthesis. There is increasing demand for the development

of efficient synthetic strategies that are economical and eco-friendly in the field of production of pharmaceuticals and agrochemicals. For this purpose, the synthesis of enantiomerically pure compounds using stereoselective hybrid systems is an attractive approach. However, most methods rely primarily on the use of enzymes, proteins, or RNA. DNA hybrid catalysis is a promising alternative because of the unique chirality of DNA and its capability to influence the stereochemical course of a reaction. Moreover, DNA-based catalytic systems can be used in aqueous media. DNA-based hybrid catalysts that self-assemble from DNA and a metal complex with a specific ligand using supramolecular or covalent anchoring strategies have high stereoselectivity and exhibit rate enhancement in Lewis acid catalyzed reactions, such as Diels–Alder, Michael addition, and Friedel–Crafts reactions.[73] However, despite a number of reports on the enantioselectivity of the reactions originated from DNA, the mechanism underlying stereoinduction remains poorly understood. Therefore, we used an intramolecular reaction as a suitable system to investigate the stereoinduction mechanism underlying DNA-based asymmetric synthesis, as it significantly reduces conformational freedom. Moreover, the Friedel–Crafts reaction was used as a model for the intramolecular reaction. We then deciphered DNA-based asymmetric catalysis through intramolecular Friedel–Crafts alkylation and proposed a plausible binding model and (*S*)-enantiomer complex with Cu(5,6-dmp) based on the intercalation.[73a] We carried out computational studies to investigate the origin of the enantioselectivity of the intramolecular Friedel–Crafts reaction, which is catalyzed by a supramolecular Cu/DNA catalyst (Figure 15a).

We modeled 28 conformations of the supramolecular L-Cu(II)-R/d(CAAAAATTTTTG)$_2$ complex and evaluated their stability and structural features according to the metal complex conformation and its intercalation position.[73b] The results suggested that *S*-product selectivity is caused by the higher binding energy of the pro-*S* conformation. Furthermore, the pro-*S* conformation appeared to be structurally closer to the TS of C3–C2′ bond formation. Consequently, we devised an advanced DNA-based hybrid catalyst based on the direct incorporation of a ligand into the DNA phosphate backbone. We successfully performed asymmetric intramolecular Friedel–Crafts alkylations using the developed DNA-based hybrid catalyst containing an intrastrand bipyridine (Figure 15b). Further investigation of the structural details of DNA hybrid catalysts via the generation of a series of active site showed that the catalytic properties are managed by (i) the disposition of the metal-binding site in the DNA duplex, (ii) the size of catalytic cavity, and (iii) the composition of nucleobases in the catalytic pocket.

An affordable and easy-to-prepare solid-supported DNA system termed **st-DNA/S1** was developed. We successfully carried out the Diels–Alder reaction and demonstrated that this system could be reused readily for 10 cycles (Figure 15c).[74a] This first-ever report of the development of a solid-supported DNA system may contribute as a valuable stepping-stone for the industrial application of DNA-based asymmetric synthesis, such as a continuous flow system. Inspired by the superior characteristics of the naturally occurring metalloenzymes in catalyzing biologically essential chemical reactions, we developed DNA metalloenzymes that combine metal-assisted catalysis with a chiral biomacromolecule. Using our DNA metalloenzymes, we successfully catalyzed asymmetric Diels–Alder reactions with high conversion, excellent endo/exo selectivity, and enantioselectivity up to −97% ee. These DNA metalloenzymes were prepared using a rational design strategy based on the Cu(II) ion, to organize the catalytic-pocket architectures, the composition of nucleobases, and the incorporation of flexible linkers (Figure 15d).[74b]

Interestingly, the DNA metalloenzymes afforded the opposite enantiomer of the Diels–Alder product compared with those obtained using a supramolecular Cu(II)–dmbpy/st–DNA catalyst system. This strategy allowed development of artificial metalloenzymes without the incorporation of an artificial binding ligand and obviated the conventional protein–metalloenzyme complexes, thus providing a new outlook on the harnessing of the catalytic repertoire of nucleic acids.

6. Summary and Outlook

There is a growing demand for the development of next-generation biomaterials that are capable of overcoming current economic, clinical and efficiency issues. A closer look at the natural cellular environment may inspire the development of novel biomaterials that are useful for humankind. We have been making steadfast progress toward the use of the chemical biology of nucleic acids to design and construct nature-inspired smart biomaterials. Recent high-throughput sequencing technologies have aided the identification of critical DNA sequences and their association with key transcription factors (TFs) that govern the expression of therapeutically important and cell-fate-governing genes. We have successfully mimicked natural TFs encompassing functional domains (repressor or activator domains) and DNA-binding domains (DBDs) to construct synthetic transcription factors. Pyrrole-imidazole polyamides (PIPs) mimicked the DBD and were capable of selectively altering the expression of therapeutically important genes, such as *EVI1*. We supplemented PIPs with DNA-alkylating agents to mimic the repressor domain of TFs and showed the site-selective repression of several oncogenes, such as *KRAS*. To mimic the activation domain, we conjugated PIPs with epigenetic activators such as SAHA and CTB. PIPs conjugated with fluorophores were used to recognize human telomeric DNA selectively. The functional components of artificial TFs were successfully altered with substantial tunability. Our collaborative studies demonstrated the pharmacokinetic properties of PIPs, suggesting the possibility of developing these artificial TFs as drugs. Next-generation sequencing studies guided the construction of advanced PIPs. We carried out mechanistic investigations to obtain a broader understanding of the structural and molecular recognition properties of biologically significant DNA conformational changes, such as G-quadruplex formation and Z-DNA formation. In particular, we proposed a new folding pathway leading to G-quadruplex formation. We also developed photoproducts that mirrored the nucleic acid local structure, to probe conformational changes at sequence resolution during irradiation. Because of its programmable self-assembling feature and precise recognition ability, DNA also represents an exceptional working material. We harnessed the DNA self-assembly system to visualize single-molecule interactions, conformational changes, and chemical/

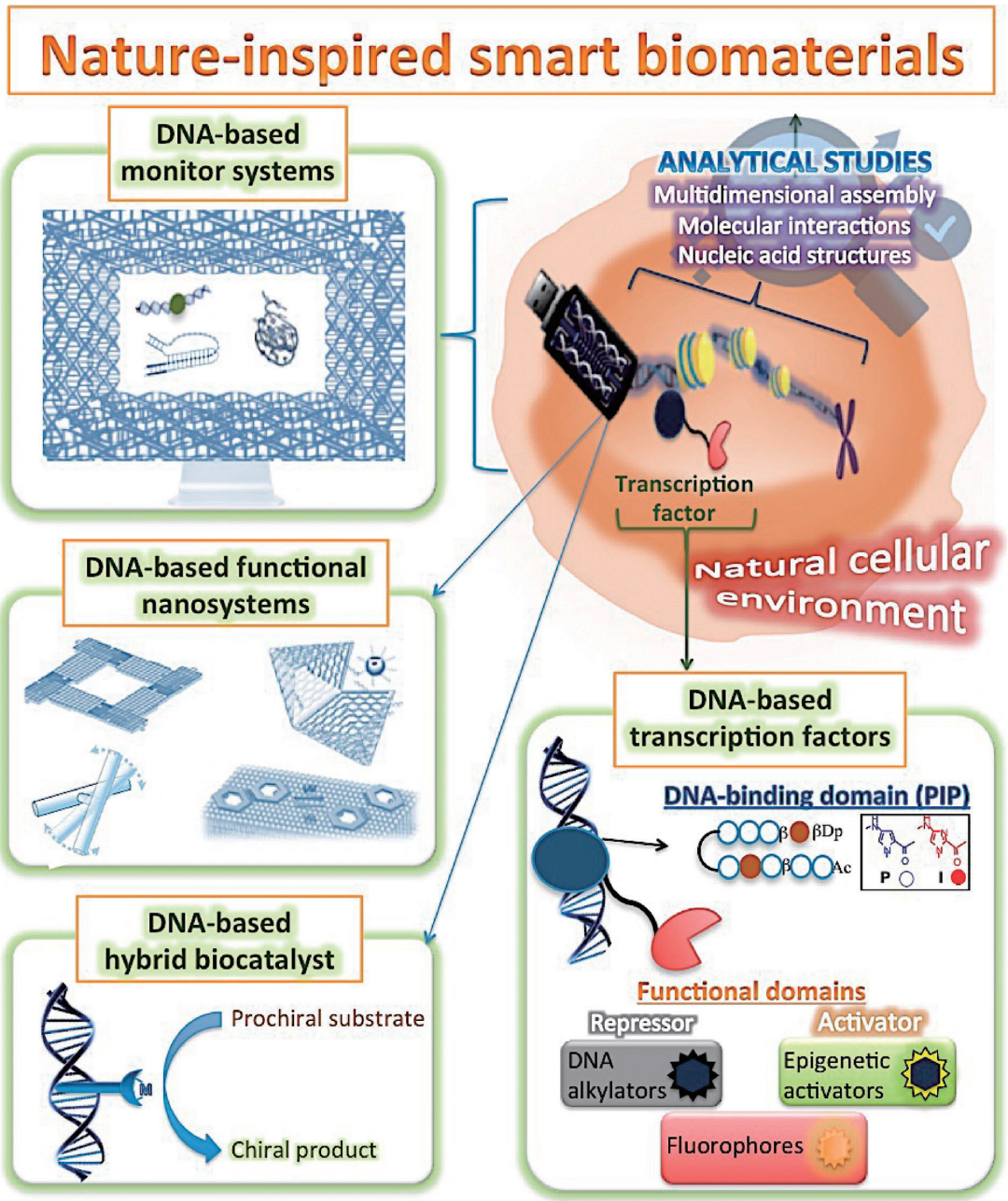

Figure 16. Schematic summary of the nature-inspired smart biomaterials constructed based on the nucleic acids and other components occurring in the natural cellular environment.

enzymatic reactions in a mimicked nanospace. We achieved an innovatively programmed assembly of nanostructures with different dimensions, to mimic the intricate structures observed in nature. We also constructed molecular nanosystems and nanodevices with versatile biological applications and developed DNA-based switching devices, such as the visible thermometer. An efficient DNA-based hybrid biocatalyst was also developed to perform asymmetric Diels–Alder and Friedel–Crafts reactions. In particular, we developed nature-inspired DNA metalloenzymes that are capable of catalyzing useful chemical reactions.

In summary, we have successfully mimicked nucleic acid and molecular components occurring in the natural cellular environment and have constructed DNA-based transcription factors, monitor systems, functional nanosystems/nanodevices and hybrid biocatalyst for versatile uses (Figure 16). Modern profiling and analytical techniques aid to attain detailed information about the nucleic acid structures that are observed in the natural cellular environment and devise innovative strategies to construct smart biomaterials for versatile applications.

References

1 G. N. Pandian, H. Sugiyama, *Pharmaceuticals* **2013**, *6*, 1.
2 J. D. Watson, *Science* **1990**, *248*, 44.
3 a) L. Chin, J. N. Anderson, P. A. Futreal, *Nat. Med.* **2011**, *17*, 297. b) G. N. Pandian, J. Taniguchi, H. Sugiyama, *Clin. Transl.*

Med. **2014**, *3*, 6. c) G. N. Pandian, J. Syed, H. Sugiyama, *Synthetic Strategies to Identify and Regulate Noncoding RNAs*, in *Long Noncoding RNAs*, Springer, **2015**, pp. 23–43. doi:10.1007/978-4-431-55576-6_2.

4 a) G. N. Pandian, R. D. Taylor, S. Junetha, A. Saha, C. Anandhakumar, T. Vaijayanthi, H. Sugiyama, *Biomater. Sci.* **2014**, *2*, 1043. b) S. Masuda, J. Wu, T. Hishida, G. N. Pandian, H. Sugiyama, J. C. I. Belmonte, *J. Mol. Cell Biol.* **2013**, *5*, 354. c) Y.-L. Wu, G. N. Pandian, Y.-P. Ding, W. Zhang, Y. Tanaka, H. Sugiyama, *Chem. Biol.* **2013**, *20*, 1311.

5 G. N. Pandian, H. Sugiyama, *Targeted Editing of Therapeutic Genes using DNA-Based Transcriptional Activators: Scope and Challenges*, in *Chemical Biology of Nucleic Acids: Fundamentals and Clinical Applications*, Springer, **2014**, pp. 347–365. doi:10.1007/978-3-642-54452-1_19.

6 S. Patel, D. Jung, P. T. Yin, P. Carlton, M. Yamamoto, T. Bando, H. Sugiyama, K.-B. Lee, *ACS Nano* **2014**, *8*, 8959.

7 G. N. Pandian, H. Sugiyama, *Biotechnol. J.* **2012**, *7*, 798.

8 Y. Xu, H. Sugiyama, *Angew. Chem., Int. Ed.* **2006**, *45*, 1354.

9 M. Endo, H. Sugiyama, *ChemBioChem* **2009**, *10*, 2420.

10 a) X. Li, D. R. Liu, *Angew. Chem., Int. Ed.* **2004**, *43*, 4848. b) K. Gorska, N. Winssinger, *Angew. Chem., Int. Ed.* **2013**, *52*, 6820.

11 J. J. Storhoff, C. A. Mirkin, *Chem. Rev.* **1999**, *99*, 1849.

12 N. C. Seeman, *Nature* **2003**, *421*, 427.

13 S. Park, H. Sugiyama, *Angew. Chem., Int. Ed.* **2010**, *49*, 3870.

14 U. Wähnert, Ch. Zimmer, G. Luck, Ch. Pitra, *Nucleic Acids Res.* **1975**, *2*, 391.

15 M. L. Kopka, C. Yoon, D. Goodsell, P. Pjura, R. E. Dickerson, *J. Mol. Biol.* **1985**, *183*, 553.

16 M. Mrksich, P. B. Dervan, *J. Am. Chem. Soc.* **1995**, *117*, 3325.

17 S. White, J. W. Szewczyk, J. M. Turner, E. E. Baird, P. B. Dervan, *Nature* **1998**, *391*, 468.

18 a) C. F. Hsu, P. B. Dervan, *Bioorg. Med. Chem. Lett.* **2008**, *18*, 5851. b) S. Nishijima, K. Shinohara, T. Bando, M. Minoshima, G. Kashiwazaki, H. Sugiyama, *Bioorg. Med. Chem.* **2010**, *18*, 978.

19 T. Vaijayanthi, T. Bando, G. N. Pandian, H. Sugiyama, *ChemBioChem* **2012**, *13*, 2170.

20 a) T. Bando, J. Fujimoto, M. Minoshima, K. Shinohara, S. Sasaki, G. Kashiwazaki, M. Mizumura, H. Sugiyama, *Bioorg. Med. Chem.* **2007**, *15*, 6937. b) J. Fujimoto, T. Bando, M. Minoshima, S. Uchida, M. Iwasaki, K. Shinohara, H. Sugiyama, *Bioorg. Med. Chem.* **2008**, *16*, 5899.

21 J. Fujimoto, T. Bando, M. Minoshima, G. Kashiwazaki, S. Nishijima, K. Shinohara, H. Sugiyama, *Bioorg. Med. Chem.* **2008**, *16*, 9741.

22 M. Minoshima, T. Bando, S. Sasaki, K. Shinohara, T. Shimizu, J. Fujimoto, H. Sugiyama, *J. Am. Chem. Soc.* **2007**, *129*, 5384.

23 T. Vaijayanthi, T. Bando, K. Hashiya, G. N. Pandian, H. Sugiyama, *Bioorg. Med. Chem.* **2013**, *21*, 852.

24 a) Y.-M. Lai, N. Fukuda, T. Ueno, H. Matsuda, S. Saito, K. Matsumoto, H. Ayame, T. Bando, H. Sugiyama, H. Mugishima, K. Serie, *J. Pharmacol. Exp. Ther.* **2005**, *315*, 571. b) Y. Kawamoto, T. Bando, F. Kamada, Y. Li, K. Hashiya, K. Maeshima, H. Sugiyama, *J. Am. Chem. Soc.* **2013**, *135*, 16468. c) A. Hirata, K. Nokihara, Y. Kawamoto, T. Bando, A. Sasaki, S. Ide, K. Maeshima, T. Kasama, H. Sugiyama, *J. Am. Chem. Soc.* **2014**, *136*, 11546. d) Y. Kawamoto, A. Sasaki, K. Hashiya, S. Ide, T. Bando, K. Maeshima, H. Sugiyama, *Chem. Sci.* **2015**, *6*, 2307. e) Y.-W. Han, Y. Tsunaka, H. Yokota, T. Matsumoto, G. Kashiwazaki, H. Morinaga, K. Hashiya, T. Bando, H. Sugiyama, Y. Harada, *Biomater. Sci.* **2014**, *2*, 297.

25 a) M. S. R. C. Murty, H. Sugiyama, *Biol. Pharm. Bull.* **2004**, *27*, 468. b) T. Takahashi, Y. Asami, E. Kitamura, T. Suzuki, X. Wang, J. Igarashi, A. Morohashi, Y. Shinojima, H. Kanou, K. Saito, T. Takasu, H. Nagase, Y. Harada, K. Kuroda, T. Watanabe, S. Kumamoto, T. Aoyama, Y. Matsumoto, T. Bando, H. Sugiyama, C. Yoshida-Noro, N. Fukuda, N. Hayashi, *Chem. Biol.* **2008**, *15*, 829. c) E.-H. Yao, N. Fukuda, T. Ueno, H. Matsuda, N. Nagase, Y. Matsumoto, H. Sugiyama, K. Matsumoto, *Cardiovasc. Res.* **2009**, *81*, 797. d) T. Ueno, N. Fukuda, A. Tsunemi, E. H. Yao, H. Matsuda, K. Tahira, T. Matsumoto, K. Matsumoto, Y. Matsumoto, H. Nagase, H. Sugiyama, T. Sawamura, *J. Hypertens.* **2009**, *27*, 508. e) T. Suzuki, Y. Asami, T. Takahashi, X. Wang, T. Watanabe, T. Bando, H. Sugiyama, N. Fukuda, H. Nagase, *J. Antibiot.* **2009**, *62*, 339. f) H. Matsuda, N. Fukuda, T. Ueno, M. Katakawa, X. Wang, T. Watanabe, S. Matsui, T. Aoyama, K. Saito, T. Bando, Y. Matsumoto, H. Nagase, K. Matsumoto, H. Sugiyama, *Kidney Int.* **2011**, *79*, 46. g) A. Yasuda, K. Noguchi, A. Yasuda, M. Minoshima, G. Kashiwazaki, T. Kanda, K. Katayama, J. Mitsuhashi, T. Bando, H. Sugiyama, Y. Sugimoto, *Cancer Sci.* **2011**, *102*, 2221.

26 J. Syed, G. N. Pandian, S. Sato, J. Taniguchi, A. Chandran, K. Hashiya, T. Bando, H. Sugiyama, *Chem. Biol.* **2014**, *21*, 1370.

27 A. Iguchi, N. Fukuda, T. Takahashi, T. Watanabe, H. Matsuda, H. Nagase, T. Bando, H. Sugiyama, K. Shimizu, *Biol. Pharm. Bull.* **2013**, *36*, 1152.

28 M. Minoshima, T. Bando, S. Sasaki, J. Fujimoto, H. Sugiyama, *Nucleic Acids Res.* **2008**, *36*, 2889.

29 a) T. Nagashima, T. Aoyama, T. Yokoe, A. Fukasawa, N. Fukuda, T. Ueno, H. Sugiyama, H. Nagase, Y. Matsumoto, *Biol. Pharm. Bull.* **2009**, *32*, 921. b) A. Fukasawa, T. Aoyama, T. Nagashima, N. Fukuda, T. Ueno, H. Sugiyama, H. Nagase, H. Matsumoto, *Biopharm. Drug Dispos.* **2009**, *30*, 81. c) T. Nagashima, T. Aoyama, A. Fukasawa, S. Watabe, N. Fukuda, T. Ueno, H. Sugiyama, H. Nagase, Y. Matsumoto, *J. Chromatogr. B: Anal. Technol. Biomed. Life Sci.* **2009**, *877*, 1070.

30 X. Wang, H. Nagase, T. Watanabe, H. Nobusue, T. Suzuki, Y. Asami, Y. Shinojima, H. Kawashima, K. Takagi, R. Mishra, J. Igarashi, M. Kimura, T. Takayama, N. Fukuda, H. Sugiyama, *Cancer Sci.* **2010**, *101*, 759.

31 H. Sugiyama, C. Lian, M. Isomura, I. Saito, A. H.-J. Wang, *Proc. Natl. Acad. Sci. U.S.A.* **1996**, *93*, 14405.

32 a) T. Bando, H. Sugiyama, *Acc. Chem. Res.* **2006**, *39*, 935. b) T. Bando, M. Minoshima, G. Kashiwazaki, K. Shinohara, S. Sasaki, J. Fujimoto, A. Ohtsuki, M. Murakami, S. Nakazono, H. Sugiyama, *Bioorg. Med. Chem.* **2008**, *16*, 2286. c) S. Sasaki, T. Bando, M. Minoshima, K. Shinohara, H. Sugiyama, *Chem.—Eur. J.* **2008**, *14*, 864. d) M. Minoshima, T. Bando, K. Shinohara, G. Kashiwazaki, S. Nishijima, H. Sugiyama, *Bioorg. Med. Chem.* **2010**, *18*, 1236. e) S. Asamitsu, Y. Kawamoto, F. Hashiya, K. Hashiya, M. Yamamoto, S. Kizaki, T. Bando, H. Sugiyama, *Bioorg. Med. Chem.* **2014**, *22*, 4646.

33 a) K. Shinohara, T. Bando, H. Sugiyama, *Anti-Cancer Drugs* **2010**, *21*, 228. b) G. Kashiwazaki, T. Bando, K. Shinohara, M. Minoshima, S. Nishijima, H. Sugiyama, *Bioorg. Med. Chem.* **2009**, *17*, 1393. c) G. Kashiwazaki, T. Bando, K. Shinohara, M. Minoshima, H. Kumamoto, S. Nishijima, H. Sugiyama, *Bioorg. Med. Chem.* **2010**, *18*, 2887. d) M. Yamamoto, T. Bando, Y. Kawamoto, R. D. Taylor, K. Hashiya, H. Sugiyama, *Bioconjugate*

Chem. **2014**, *25*, 552. e) C. Guo, Y. Kawamoto, S. Asamitsu, Y. Sawatani, K. Hashiya, T. Bando, H. Sugiyama, *Bioorg. Med. Chem.* **2015**, *23*, 855.

34 a) M. Minoshima, J. C. Chou, S. Lefebvre, T. Bando, K. Shinohara, J. M. Gottesfeld, H. Sugiyama, *Bioorg. Med. Chem.* **2010**, *18*, 168. b) G. Kashiwazaki, T. Bando, T. Yoshidome, S. Masui, T. Takagaki, K. Hashiya, G. N. Pandian, J. Yasuoka, K. Akiyoshi, H. Sugiyama, *J. Med. Chem.* **2012**, *55*, 2057.

35 a) R. D. Taylor, S. Asamitsu, T. Takenaka, M. Yamamoto, K. Hashiya, Y. Kawamoto, T. Bando, H. Nagase, H. Sugiyama, *Chem.—Eur. J.* **2014**, *20*, 1310. b) K. Hiraoka, T. Inoue, R. D. Taylor, T. Watanabe, N. Koshikawa, H. Yoda, K. Shinohara, A. Takatori, K. Sugimoto, Y. Maru, T. Denda, K. Fujiwara, A. Balmain, T. Ozaki, T. Bando, H. Sugiyama, H. Nagase, *Nat. Commun.* **2015**, *6*, 6706. c) R. D. Taylor, A. Chandran, G. Kashiwazaki, K. Hashiya, T. Bando, H. Nagase, H. Sugiyama, *Chem.—Eur. J.* **2015**, *21*, 14996.

36 a) Y.-W. Han, T. Matsumoto, H. Yokota, G. Kashiwazaki, H. Morinaga, K. Hashiya, T. Bando, Y. Harada, H. Sugiyama, *Nucleic Acids Res.* **2012**, *40*, 11510. b) Y.-W. Han, G. Kashiwazaki, H. Morinaga, T. Matsumoto, K. Hashiya, T. Bando, H. Sugiyama, *Bioorg. Med. Chem.* **2013**, *21*, 5436. c) W. Zhang, S.-K. Jiang, Y.-L. Wu, C.-X. Guo, H.-F. Zhang, H. Sugiyama, X.-L. Chen, *ChemBioChem* **2012**, *13*, 47. d) R. D. Taylor, Y. Kawamoto, K. Hashiya, T. Bando, H. Sugiyama, *Chem.—Asian J.* **2014**, *9*, 2527.

37 a) S. Park, T. Bando, K. Shinohara, S. Nishijima, H. Sugiyama, *Bioconjugate Chem.* **2011**, *22*, 120. b) T. Takagaki, T. Bando, M. Kitano, K. Hashiya, G. Kashiwazaki, H. Sugiyama, *Bioorg. Med. Chem.* **2011**, *19*, 5896. c) T. Takagaki, T. Bando, H. Sugiyama, *J. Am. Chem. Soc.* **2012**, *134*, 13074. d) W. Kameshima, T. Ishizuka, M. Minoshima, M. Yamamoto, H. Sugiyama, Y. Xu, M. Komiyama, *Angew. Chem., Int. Ed.* **2013**, *52*, 13681.

38 a) H. Morinaga, T. Bando, T. Takagaki, M. Yamamoto, K. Hashiya, H. Sugiyama, *J. Am. Chem. Soc.* **2011**, *133*, 18924. b) M. Yamamoto, T. Bando, N. Morinaga, Y. Kawamoto, K. Hashiya, H. Sugiyama, *Chem.—Eur. J.* **2014**, *20*, 752.

39 A. Ohtsuki, M. T. Kimura, M. Minoshima, T. Suzuki, M. Ikeda, T. Bando, H. Nagase, K. Shinohara, H. Sugiyama, *Tetrahedron Lett.* **2009**, *50*, 7288.

40 a) G. N. Pandian, K. Shinohara, A. Ohtsuki, Y. Nakano, M. Minoshima, T. Bando, H. Nagase, Y. Yamada, A. Watanabe, N. Terada, S. Sato, H. Morinaga, H. Sugiyama, *ChemBioChem* **2011**, *12*, 2822. b) G. N. Pandian, Y. Nakano, S. Sato, H. Morinaga, T. Bando, H. Nagase, H. Sugiyama, *Sci. Rep.* **2012**, *2*, 544.

41 a) G. N. Pandian, J. Taniguchi, S. Junetha, S. Sato, L. Han, A. Saha, C. AnandhaKumar, T. Bando, H. Nagase, T. Vaijayanthi, R. D. Taylor, H. Sugiyama, *Sci. Rep.* **2014**, *4*, 3843. b) L. Han, G. N. Pandian, S. Junetha, S. Sato, C. AnandhaKumar, J. Taniguchi, A. Saha, T. Bando, H. Nagase, H. Sugiyama, *Angew. Chem., Int. Ed.* **2013**, *52*, 13410. c) G. N. Pandian, S. Sato, C. AnandhaKumar, J. Taniguchi, K. Takashima, J. Syed, L. Han, A. Saha, T. Bando, H. Nagase, H. Sugiyama, *ACS Chem. Biol.* **2014**, *9*, 2729. d) J. Syed, A. Chandran, G. N. Pandian, J. Taniguchi, S. Sato, K. Hashiya, G. Kashiwazaki, T. Bando, H. Sugiyama, *ChemBioChem* **2015**, *16*, 1497.

42 a) G. N. Pandian, A. Ohtsuki, T. Bando, S. Sato, K. Hashiya, H. Sugiyama, *Bioorg. Med. Chem.* **2012**, *20*, 2656. b) A. Saha, G. N. Pandian, S. Sato, J. Taniguchi, K. Hashiya, T. Bando, H. Sugiyama, *Bioorg. Med. Chem.* **2013**, *21*, 4201. c) A. Saha, G. N. Pandian, S. Sato, J. Taniguchi, Y. Kawamoto, K. Hashiya, T. Bando, H. Sugiyama, *ChemMedChem* **2014**, *9*, 2374.

43 a) C. AnandhaKumar, Y. Li, S. Kizaki, G. N. Pandian, K. Hashiya, T. Bando, H. Sugiyama, *ChemBioChem* **2014**, *15*, 2647. b) C. AnandhaKumar, S. Kizaki, T. Bando, G. N. Pandian, H. Sugiyama, *ChemBioChem* **2015**, *16*, 20.

44 a) L. Han, G. N. Pandian, A. Chandran, S. Sato, J. Taniguchi, G. Kashiwazaki, Y. Sawatani, K. Hashiya, T. Bando, Y. Xu, X. Qian, H. Sugiyama, *Angew. Chem., Int. Ed.* **2015**, *54*, 8700. b) S. Patel, T. Pongkulapa, P. T. Yin, G. N. Pandian, C. Rathnam, T. Bando, T. Vaijayanthi, H. Sugiyama, K.-B. Lee, *J. Am. Chem. Soc.* **2015**, *137*, 4598.

45 N. Mulholland, Y. Xu, H. Sugiyama, K. Zhao, *Cell Biosci.* **2012**, *2*, 3.

46 a) Y. Xu, H. Sato, Y. Sannohe, K. Shinohara, H. Sugiyama, *J. Am. Chem. Soc.* **2008**, *130*, 16470. b) Y. Sannohe, K. Sato, A. Matsugami, K. Shinohara, T. Mashimo, M. Katahira, H. Sugiyama, *Bioorg. Med. Chem.* **2009**, *17*, 1870.

47 a) T. Mashimo, H. Yagi, Y. Sannohe, A. Rajendran, H. Sugiyama, *J. Am. Chem. Soc.* **2010**, *132*, 14910. b) D. Koirala, T. Mashimo, Y. Sannohe, Z. Yu, H. Mao, H. Sugiyama, *Chem. Commun.* **2012**, *48*, 2006. c) D. Koirala, C. Ghimire, C. Bohrer, Y. Sannohe, H. Sugiyama, H. Mao, *J. Am. Chem. Soc.* **2013**, *135*, 2235.

48 a) D. Koirala, S. Dhakal, B. Ashbridge, Y. Sannohe, R. Rodriguez, H. Sugiyama, S. Balasubramanian, H. Mao, *Nat. Chem.* **2011**, *3*, 782. b) C. Ghimire, S. Park, K. Iida, P. Yangyuoru, H. Otomo, Z. Yu, K. Nagasawa, H. Sugiyama, H. Mao, *J. Am. Chem. Soc.* **2014**, *136*, 15537.

49 a) H. Sugiyama, *Bull. Chem. Soc. Jpn.* **2007**, *80*, 823. b) R. Tashiro, K. Nakamura, H. Sugiyama, *Tetrahedron Lett.* **2008**, *49*, 428. c) R. Tashiro, A. Ohtsuki, H. Sugiyama, *J. Am. Chem. Soc.* **2010**, *132*, 14361. d) Y. Sannohe, S. Kizaki, S. Kanesato, A. Fujiwara, Y. Li, H. Morinaga, R. Tashiro, H. Sugiyama, *Chem.—Eur. J.* **2014**, *20*, 1223. e) Y. Li, H. Sugiyama, *Chem. Commun.* **2015**, *51*, 8861.

50 H. Morinaga, S. Kizaki, T. Takenaka, S. Kanesato, Y. Sannohe, R. Tashiro, H. Sugiyama, *Bioorg. Med. Chem.* **2013**, *21*, 466.

51 a) H. Morinaga, T. Takenaka, F. Hashiya, S. Kizaki, K. Hashiya, T. Bando, H. Sugiyama, *Nucleic Acids Res.* **2013**, *41*, 4724. b) F. Hashiya, A. Saha, S. Kizaki, Y. Li, H. Sugiyama, *Nucleic Acids Res.* **2014**, *42*, 13469. c) A. Saha, F. Hashiya, S. Kizaki, S. Asamitsu, K. Hashiya, T. Bando, H. Sugiyama, *Chem. Commun.* **2015**, *51*, 14485.

52 P. W. K. Rothemund, *Nature* **2006**, *440*, 297.

53 a) M. Endo, Y. Katsuda, K. Hidaka, H. Sugiyama, *J. Am. Chem. Soc.* **2010**, *132*, 1592. b) M. Endo, Y. Katsuda, K. Hidaka, H. Sugiyama, *Angew. Chem., Int. Ed.* **2010**, *49*, 9412. c) M. Endo, K. Tatsumi, K. Terushima, Y. Katsuda, K. Hidaka, Y. Harada, H. Sugiyama, *Angew. Chem., Int. Ed.* **2012**, *51*, 8778. d) M. Endo, Y. Takeuchi, Y. Suzuki, T. Emura, K. Hidaka, F. Wang, I. Willner, H. Sugiyama, *Angew. Chem., Int. Ed.* **2015**, *54*, 10550. e) S. Yamamoto, D. De, K. Hidaka, K. K. Kim, M. Endo, H. Sugiyama, *Nano Lett.* **2014**, *14*, 2286.

54 a) S. Kizaki, H. Sugiyama, *Org. Biomol. Chem.* **2014**, *12*, 104. b) S. Kizaki, Y. Suzuki, T. Takenaka, M. Endo, H. Sugiyama, *Biomater. Sci.* **2014**, *2*, 1399.

55 a) T. Yoshidome, M. Endo, G. Kashiwazaki, K. Hidaka, T. Bando, H. Sugiyama, *J. Am. Chem. Soc.* **2012**, *134*, 4654. b) E. Nakata, F. F. Liew, C. Uwatoko, S. Kiyonaka, Y. Mori, Y. Katsuda, M. Endo, H. Sugiyama, T. Morii, *Angew. Chem., Int. Ed.* **2012**, *51*, 2421.

56 a) Y. Suzuki, M. Endo, Y. Katsuda, K. Ou, K. Hidaka, H. Sugiyama, *J. Am. Chem. Soc.* **2014**, *136*, 211. b) Y. Suzuki, M. Endo, C. Cañas, S. Ayora, J. C. Alonso, H. Sugiyama, K. Takeyasu, *Nucleic Acids Res.* **2014**, *42*, 7421.

57 a) M. Endo, Y. Yang, Y. Suzuki, K. Hidaka, H. Sugiyama, *Angew. Chem., Int. Ed.* **2012**, *51*, 10518. b) Y. Takeuchi, M. Endo, Y. Suzuki, K. Hidaka, G. Durand, E. Dausse, J.-J. Toulmé, H. Sugiyama, *Biomater. Sci.* **2016**, *4*, 130.

58 a) M. Endo, M. Inoue, Y. Suzuki, C. Masui, H. Morinaga, K. Hidaka, H. Sugiyama, *Chem.—Eur. J.* **2013**, *19*, 16887. b) A. Rajendran, M. Endo, K. Hidaka, H. Sugiyama, *J. Am. Chem. Soc.* **2013**, *135*, 1117.

59 a) Y. Sannohe, M. Endo, Y. Katsuda, K. Hidaka, H. Sugiyama, *J. Am. Chem. Soc.* **2010**, *132*, 16311. b) Y. Yang, M. Endo, Y. Suzuki, K. Hidaka, H. Sugiyama, *Chem. Commun.* **2014**, *50*, 4211. c) M. Endo, X. Xing, X. Zhou, T. Emura, K. Hidaka, B. Tuesuwan, H. Sugiyama, *ACS Nano* **2015**, *9*, 9922.

60 a) A. Rajendran, M. Endo, K. Hidaka, P. L. T. Tran, J.-L. Mergny, H. Sugiyama, *Nucleic Acids Res.* **2013**, *41*, 8738. b) A. Rajendran, M. Endo, K. Hidaka, P. L. T. Tran, J.-L. Mergny, R. J. Gorelick, H. Sugiyama, *J. Am. Chem. Soc.* **2013**, *135*, 18575. c) A. Rajendran, M. Endo, K. Hidaka, P. L. T. Tran, M.-P. Teulade-Fichou, J.-L. Mergny, H. Sugiyama, *RSC Adv.* **2014**, *4*, 6346.

61 a) A. Rajendran, M. Endo, K. Hidaka, H. Sugiyama, *Angew. Chem., Int. Ed.* **2014**, *126*, 4191. b) A. Rajendran, M. Endo, K. Hidaka, M.-P. Teulade-Fichou, J.-L. Mergny, H. Sugiyama, *Chem. Commun.* **2015**, *51*, 9181.

62 M. Endo, K. Hidaka, T. Kato, K. Namba, H. Sugiyama, *J. Am. Chem. Soc.* **2009**, *131*, 15570.

63 a) M. Endo, T. Sugita, Y. Katsuda, K. Hidaka, H. Sugiyama, *Chem.—Eur. J.* **2010**, *16*, 5362. b) M. Endo, T. Sugita, A. Rajendran, Y. Katsuda, T. Emura, K. Hidaka, H. Sugiyama, *Chem. Commun.* **2011**, *47*, 3213. c) A. Rajendran, M. Endo, Y. Katsuda, K. Hidaka, H. Sugiyama, *ACS Nano* **2011**, *5*, 665. d) A. Rajendran, M. Endo, K. Hidaka, H. Sugiyama, *Chem. Commun.* **2013**, *49*, 686.

64 a) L. A. Yatsunyk, O. Piétrement, D. Albrecht, P. L. T. Tran, D. Renčiuk, H. Sugiyama, J.-M. Arbona, J.-P. Aimé, J.-L. Mergny, *ACS Nano* **2013**, *7*, 5701. b) M. Endo, S. Yamamoto, T. Emura, K. Hidaka, N. Morone, J. E. Heuser, H. Sugiyama, *Angew. Chem., Int. Ed.* **2014**, *53*, 7484. c) M. Endo, S. Yamamoto, K. Tatsumi, T. Emura, K. Hidaka, H. Sugiyama, *Chem. Commun.* **2013**, *49*, 2879. d) A. Rajendran, M. Endo, K. Hidaka, N. Shimada, A. Maruyama, H. Sugiyama, *Chem. Commun.* **2014**, *50*, 8743. e) M. Endo, K. Hidaka, H. Sugiyama, *Org. Biomol. Chem.* **2011**, *9*, 2075.

65 a) S. F. J. Wickham, M. Endo, Y. Katsuda, K. Hidaka, J. Bath, H. Sugiyama, A. J. Turberfield, *Nat. Nanotechnol.* **2011**, *6*, 166. b) S. F. J. Wickham, J. Bath, Y. Katsuda, M. Endo, K. Hidaka, H. Sugiyama, A. J. Tuberfield, *Nat. Nanotechnol.* **2012**, *7*, 169.

66 a) M. Endo, Y. Yang, T. Emura, K. Hidaka, H. Sugiyama, *Chem. Commun.* **2011**, *47*, 10743. b) D. Koirala, P. Shrestha, T. Emura, K. Hidaka, S. Mandal, M. Endo, H. Sugiyama, H. Mao, *Angew. Chem., Int. Ed.* **2014**, *126*, 8275. c) R. Tashiro, M. Iwamoto, H. Morinaga, T. Emura, K. Hidaka, M. Endo, H. Sugiyama, *Nucleic Acids Res.* **2015**, *25*, 245. d) M. Endo, R. Miyazaki, T. Emura, K. Hidaka, H. Sugiyama, *J. Am. Chem. Soc.* **2012**, *134*, 2852.

67 a) A. Rajendran, M. Endo, Y. Katsuda, K. Hidaka, H. Sugiyama, *J. Am. Chem. Soc.* **2011**, *133*, 14488. b) Y. Yang, M. Endo, K. Hidaka, H. Sugiyama, *J. Am. Chem. Soc.* **2012**, *134*, 20645. c) Y. Suzuki, M. Endo, Y. Yang, H. Sugiyama, *J. Am. Chem. Soc.* **2014**, *136*, 1714. d) T. Takenaka, M. Endo, Y. Suzuki, Y. Yang, T. Emura, K. Hidaka, T. Kato, T. Mitata, K. Namba, H. Sugiyama, *Chem.—Eur. J.* **2014**, *20*, 14951. e) Y. Yang, M. A. Goetzfried, K. Hidaka, M. You, W. Tan, H. Sugiyama, M. Endo, *Nano Lett.* **2015**, *15*, 6672.

68 a) K. Mohri, M. Nishikawa, N. Takahashi, T. Shiomi, N. Matsuoka, K. Ogawa, M. Endo, K. Hidaka, H. Sugiyama, Y. Takahashi, Y. Takakura, *ACS Nano* **2012**, *6*, 5931. b) T. Yata, Y. Takahashi, M. Tan, K. Hidaka, H. Sugiyama, M. Endo, Y. Takakura, M. Nishikawa, *Sci. Rep.* **2015**, *5*, 14979. c) Y. Nishida, S. Ohtsuki, Y. Araie, Y. Umeki, M. Endo, T. Emura, K. Hidaka, H. Sugiyama, Y. Takahashi, Y. Takakura, M. Nishikawa, *Nanomedicine (N. Y., NY, U. S.)* **2016**, *12*, 123.

69 E. Osada, Y. Suzuki, K. Hidaka, H. Ohno, H. Sugiyama, M. Endo, H. Saito, *ACS Nano* **2014**, *8*, 8130.

70 Y. Suzuki, M. Endo, H. Sugiyama, *Nat. Commun.* **2015**, *6*, 8052.

71 Y. Sannohe, H. Sugiyama, *Bioorg. Med. Chem.* **2012**, *20*, 2030.

72 a) H. Otomo, S. Park, S. Yamamoto, H. Sugiyama, *RSC Adv.* **2014**, *4*, 31341. b) S. Park, H. Otomo, L. Zheng, H. Sugiyama, *Chem. Commun.* **2014**, *50*, 1573. c) S. Yamamoto, S. Park, H. Sugiyama, *RSC Adv.* **2015**, *5*, 104601. d) F. Y.-H. Chen, S. Park, H. Otomo, S. Sakashita, H. Sugiyama, *Artif. DNA: PNA XNA* **2014**, *5*, e28226.

73 a) S. Park, K. Ikehata, R. Watabe, Y. Hidaka, A. Rajendran, H. Sugiyama, *Chem. Commun.* **2012**, *48*, 10398. b) G. P. Petrova, Z. Ke, S. Park, H. Sugiyama, K. Morokuma, *Chem. Phys. Lett.* **2014**, *600*, 87. c) S. Park, L. Zheng, S. Kumakiri, S. Sakashita, H. Otomo, K. Ikehata, H. Sugiyama, *ACS Catal.* **2014**, *4*, 4070.

74 a) S. Park, K. Ikehata, H. Sugiyama, *Biomater. Sci.* **2013**, *1*, 1034. b) S. Park, I. Okamura, S. Sakashita, J. H. Yum, C. Acharya, L. Gao, H. Sugiyama, *ACS Catal.* **2015**, *5*, 4708.